NTNU
Norges teknisk-naturvitenskapelige universitet

Fakultet for informasjonsteknologi, matematikk og elektroteknikk
Institutt for teknisk kybernetikk

MASTEROPPGAVE

Kandidatens navn: Jørgen Kringen Johnsen

Fag: Teknisk Kybernetikk

Oppgavens tittel (norsk): Robust destillasjonsregulering – Anvendelse av H-uendelig loop shaping

Oppgavens tittel (engelsk): Robust Distillation Control – Application of H-infinity Loop Shaping

Oppgavens tekst:

The purpose of the assignment is to design a control system for an experimental distillation column separating water and methanol. The candidate will have to make a dynamic model for simulation and controller synthesis, and also a temperature based composition estimator for composition feedback to the controller. The remaining part of the work will be to design a controller for the distillation column, and the candidate should especially look into using H_∞ loop shaping for the design of a composition controller.

The control design should be implemented on the experimental distillation column using LabView and tried out in experiments.

Oppgaven gitt: 10. januar 2005

Besvarelsen leveres: 17. juni 2005

Besvarelsen levert: 17. juni 2005

Utført ved Institutt for teknisk kybernetikk

Faglærer: Professor Morten Hovd
Veileder: Professor Sigurd Skogestad

Trondheim, den

Faglærer

Preface

This report summarizes the diploma work done on my Master of Science degree at NTNU. It has been a rewarding time, and I have enjoyed participating in building up the experimental column and to follow the project from modeling, through simulations and experimental testing. Long hours have been spent in the lab running experiments, sometimes rather tedious, but with the tediousness outweighed by the joy felt when seing the controller actually work for the first time. Nevertheless, I am glad to now hand in this report and to end the long hours — at least for a little while.

I want to express my sincere thanks to my supervisors Professor Morten Hovd at Department of Engineering Cybernetics, and Professor Sigurd Skogestad at Department of Chemical Engineering, for their helpful criticism. I thank Ingela Reppe for doing the work of getting experimental composition data for the estimator, and for bearing up with me as this project has evolved and the level of stress increased. Finally I would like to give my thanks to the other students in the office; Elise, Elisabeth, Ingrid and Marit, without whom this final year as a student would definitely not have been the same.

Trondheim, June 16th, 2005

Jørgen Kringen Johnsen

Abstract

A control system for composition control of a distillation column is developed. For simulations and controller synthesis, a simplified first-principles distillation column model is created. Model parameters are manually tuned to fit the model to data from an experimental distillation column. For composition feedback to the controller, a temperature based composition estimator is constructed from experimental data. Robustness properties of two composition controllers, a PI controller and an H_∞ loop shaping controller, are investigated. Simulations show that the H_∞ controller is more robust to input gain perturbations and time delays. The pre-compensator in the H_∞ loop shaping design is selected as a regular PI controller where controller gains are determined from the SIMC PI tuning rules. This way of selecting a pre-compensator makes loop shaping easier for the designer. Both of the controllers are successfully implemented on an experimental column.

Contents

1. Introduction

This chapter gives a brief description of the problems considered in this report and the key results presented in each chapter.

1.1 What is this report about?

Distillation is probably the most widely used separation process in the chemical and allied industries; its applications ranging from the rectification of alcohol, which has been practiced since antiquity, to the fractionation of crude oil (Sinnot, 1999). Because of its importance, distillation has been well studied over the years, several articles, ph.d. theses and books have been written on topics like column design, distillation models, product estimators and distillation control. Some of the existing theory is applied when we in this report show an implementation of a control system on a continuous distillation column. The work consists of the typical steps involved in developing a controller for any experimental setup; first modeling, then iterations of simulation and controller synthesis, and finally implementation of the controller on a real system — frequently with subsequent iterations of re-tuning and simulations. The results of the work is presented in this report.

1.2 Chapter outline

In chapter 2 we will start by looking at the experimental column we are trying to control and then describe the column instrumentation and the different control loops involved.

Next, in chapter 3, a dynamic column model is developed. Starting from first-principles conservation laws, model assumptions are introduced to simplify the various equations. The simplified column model is fitted to experimental data and used subsequently for controller synthesis and simulations.

A composition estimator is used to get feedback to the controller. Chapter 4 describes how a temperature based composition estimator is constructed from experimentally obtained composition and temperature data.

Chapter 5 is a theory chapter in which the idea of H_∞ loop shaping is presented. H_∞ loop shaping consists of two steps: First the open loop singular values are shaped by placing pre- and post-compensators before and after the plant. Second, this shaped plant

is robustified with respect to coprime factor uncertainty by adding an additional controller in the feedback path. A particulary simple method for obtaining a pre-compensator is proposed, where the diagonal elements are chosen as PI-controllers tuned by using the SIMC PI-tuning rules.

In chapter 6 theory is brought to practice, and controllers are designed for a distillation column. The improved robustness properties of the H_∞ controller compared to a conventional PI controller are shown through simulations with varying system gain and phase. While the PI controller is clearly affected by perturbing these parameters, the H_∞ controller (with PI controller as pre-compensator) shows much less performance variations with plant parameter variations. The controllers are also implemented on the experimental column, which was the overall goal of this project. Both controllers are found to perform satisfactory, as the nominal plant model matches well with the experimental column, with less parameter uncertainty than simulated in the worst case scenarios.

Finally, chapter 7 summarizes the main conclusions of the previous chapters.

2. Experimental column setup

In this chapter a short description of the different components in the experimental column is given, together with an overview of inputs to and outputs from the system. The different control loops involved in the automatic control system are presented.

2.1 The column

Figure 2.1 shows a picture of the distillation column together with a flow sheet. Table 2.1 gives the most important column data.

The column consists of two sections filled with 6mm Raschig-rings unstructured packing. A condenser is connected to the top of the column. The condensate flows into the reflux drum, from where a fraction is pumped back into the column as reflux to get desired composition. The distillate pumped out of the system and into the distillate product tank is used to control the level in the reflux drum.

Vapor is produced by heating coils in the boiler connected to the bottom of the column. The boiler level is controlled through the bottoms flow pumped out of the system and into the bottoms product tank. For security, the boiler is protected with a plexi-glass cover shield.

A feed mixture of methanol and water is pumped from the feed tank and into the feed section approximately in the center of the column. To avoid spill after finishing an experiment, a manually controlled recycle pump is used to transfer distillate and bottoms back into the feed product tank.

The entire system is mounted in an aluminum frame which can be moved as a single unit.

2.2 Instrumentation

2.2.1 Actuators

Five pumps are connected to the column system to control the different flows. The reflux and feed pumps are continuous with 4-20mA input. The distillate and bottoms pumps are on/off pumps which are pulse width modulated to allow for different pump rates.

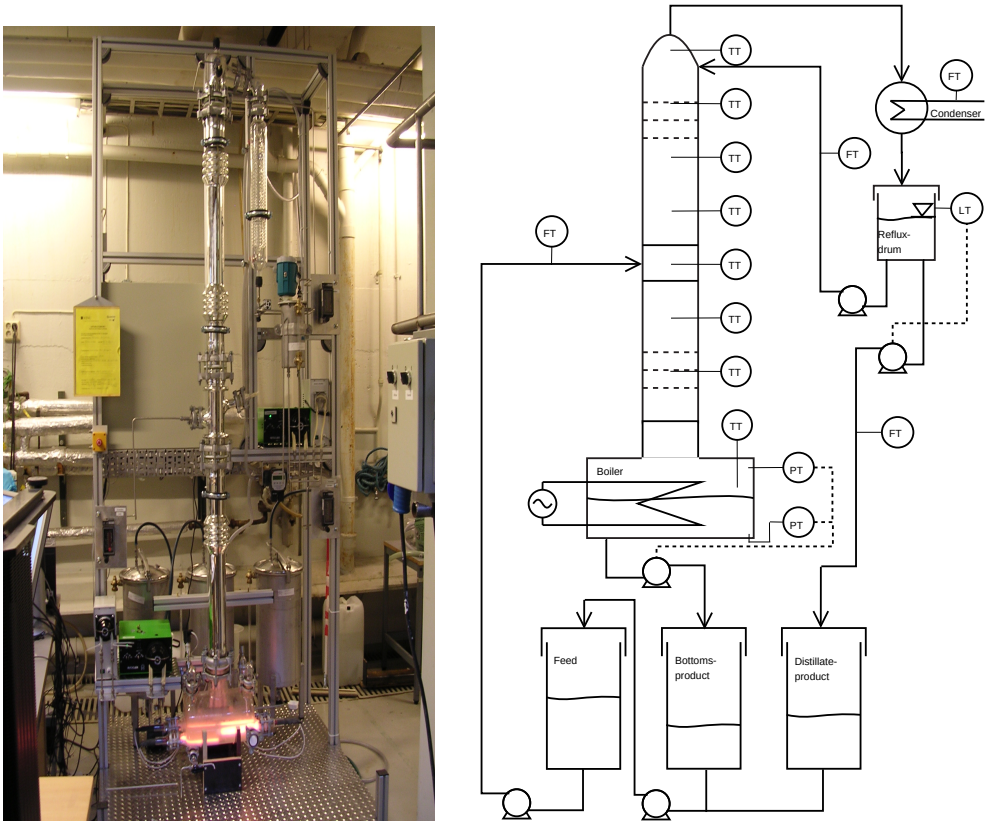

(a) Experimental setup (b) Flow sheet with sensors and actuators

Figure 2.1: Distillation system

Table 2.1: Column data

Material:	Glass and steel
Column height:	250cm
Diameter:	50mm
Condenser:	0.3m^2 i.d.
Max boiler power:	3kW
Max reflux rate:	4ml/s
Max feed rate:	5ml/s
Boiler volume:	10l
Reflux drum volume:	5l
Product tanks volume:	25l
Frame dimensions:	120 × 125 × 285cm (l×w×h)

The recycle pump is of on/off type and is turned on manually by the operator when recycling the products before a new experiment. This pump is not a part of the automatic control system.

Four heating coils generate the vapor inside the column. Two coils are 1000W each, the two other ones are 500W, giving a total of 3kW power input. The heating coils are turned on and off by relays, and are pulse width modulated.

2.2.2 Sensors

There are eight PT-100 temperature sensors inside the column to measure the temperature profile. One of the sensors is in the boiler, the remaining ones are inserted via the feed section and the top, and are held in place by the column packing. A Fieldpoint RTD I/O module measures temperature sensor resistance and converts resistance to temperature.

Two pressure sensors are located at the top and at the bottom of the boiler respectively. The pressure difference between the sensors is proportional to liquid level in the boiler and is used as input to the boiler level controller. The column is open to air after the condenser in the top, hence the absolute pressure above the liquid boiler holdup gives the pressure fall over the column.

A level sensor is placed in the reflux drum to give feedback to the reflux level controller.

The cooling water is equipped with a flow meter to assist the operator when turning on cooling. The sensor output is also monitored during operation, and warnings are issued if the cooling water for some reason should stop.

Flow meters are placed on the feed, reflux and distillate flows. These sensors gives visual feedback to the operator through displays on the sensors. They are not used as measurements in the control system for two reasons: The squeezing tube pumps produce pulsating flows which are below the measurement range of the flow meters in parts of the oscillation period. Hence the measurement signal is unsymmetrical and averaging or possibly a notch filter on the signal is not very suitable. The other reason why the flow meters are not used in the controller, is that especially the feed flow meter quite often gets stuck on a specific flow value. The flow meters use the angle of a small pendulum as a measurement proportional to mass flow rates. Small particles in the feed jam the pendulum in a certain position thereby making the measurement signal useless. Instead of using flow meters, pump characteristics are used to give estimates of the actual feed and reflux flows. To make use of the flow meters one could mount equipment like pulse dampers and filters in the piping, but at least for control it works to instead use a one to one relation between pump speed and flow rate.

2.3 Control loops

As mentioned there are two level control loops in the system. A conventional LV-configuration is used where reflux and vapor flows are used for composition control, the

level in the reflux drum is controlled through the distillate flow, and the boiler liquid level is controlled through the bottoms flow. Both of the level controllers are P-controllers where suitable gains were found by trial and error. Steady state level offsets are unimportant in this configuration, which is why no integral terms are included in the controllers.

Some logical statements are included in the control software if unexpected situations should occur. If the cooling water stops, the operator is given a warning on the screen. If the cooling waters remains off for more than five minutes, the column will be shut down. The heating coils will be turned off if the boiler level gets below a minimum value. If the column pressure increases above the saturation point of the upper pressure sensor, indicating high boiler liquid level or that significant flooding is present, the feed will be turned off to prevent more liquid from entering. No action is taken for extreme level values in the reflux drum, as no dangerous situations occur. If the drum gets full, the content will begin to fill the condenser and eventually flow back into the column. If the drum gets empty there will be no reflux available, resulting in less pure distillate. This is of course unfortunate, but not dangerous.

If all else fails, an emergency switch is placed on the aluminum frame. Pressing the emergency switch cuts the main power supply and the column will be shut down.

With level loops closed, what is left to control are the compositions of the bottoms and distillate flows. The reminder of this thesis is basically concerned with finding a way of using the two free variables; reflux flow and vapor flow, to control the concentration of methanol in the product flows.

3. Dynamic column model

In this chapter a general first-principles dynamic model of distillation columns will be derived. First a rigorous model is presented, followed by model assumptions and simplifications to reduce the model complexity. The main goal is to derive a model suitable for simulation of the experimental column presented in the previous chapter. The derivation of a rigorous non-linear model and model simplifications is mainly based on a survey paper by Skogestad (1997) and references therein. Other references are given in the text.

3.1 Rigorous model

The most common way of deriving a rigorous model of a distillation column is to divide the column into stages and include mass- and energy balances on each stage. In addition one include models of the liquid flow dynamics and possibly the pressure dynamics. Nevertheless, even with a rigorous approach, model simplifications such as assuming a thermodynamic vapor/liquid equilibrium (VLE) on each stage, are normally legible while still capturing the dynamics important for control.

For a packed column, one may question using a staged model instead of partial differential equations for describing the column dynamics. The packed column is most naturally thought of as a distributed system and accordingly it may seem natural to use PDE models. However, over the years it has been established that the dynamics of packed columns are quite similar to that of columns with trays. By adjusting the number of theoretical stages in a staged model of a packed column one can obtain models that correlates well with experimental setups. The staged model thus presents a convenient way of discretizing the system, and according to Skogestad (1997), presently there does not seem to be any clear advantages in using PDE models for distillation.

Assume a two component system (e.g. water and methanol). Let stage i represent a control volume with holdup M_i, and let the liquid flow L_i and vapor flow V_i be the flows leaving stage i with compositions x_i and y_i respectively (see figure 3.1). Mass- and energy balances for the control volume with no feed or product streams give the following set of differential and algebraic equations:

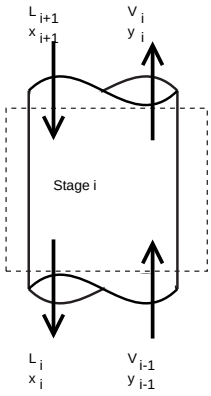

Figure 3.1: Control volume on stage i. No feed or product streams.

(i) *Component material balance (composition dynamics)*

$$\frac{d}{dt}N_i = L_{i+1}x_{i+1} - L_i x_i + V_{i-1}y_{i-1} - V_i y_i, \tag{3.1}$$

where $N_i = M_i^l x_i + M_i^v y_i$ is the molar holdup of light component on stage i in liquid phase ($M_i^l x_i$) and vapor phase ($M_i^v y_i$).

(ii) *Overall mass balance (flow dynamics)*

$$\frac{d}{dt}M_i = \frac{d}{dt}\left(M_i^l + M_i^v\right) = L_{i+1} - L_i + V_{i-1} - V_i \tag{3.2}$$

(iii) *Energy balance*

$$\frac{d}{dt}U_i = L_{i+1}h_{i+1}^l - L_i h_i^l + V_{i-1}h_{i-1}^v - V_i h_i^v, \tag{3.3}$$

where the internal energy $U_i = M_i^l u_i^l + M_i^v u_i^v$ and u and h are the specific energy and enthalpy of the different phases.

(iv) *Tray hydraulics*
The liquid and vapor flows leaving a stage is typically calculated from algebraic equations relating the flows to holdup and pressure drops:

$$L_i = f_l(M_i, V_i, \Delta P_i) \tag{3.4}$$
$$V_i = f_v(M_i, \Delta P_i). \tag{3.5}$$

For feedback control, a linear relationship between flows and liquid holdup is normally sufficient. Another approach would be to use e.g. the Francis weir formula.

(v) *Vapor-liquid equilibrium (VLE)*
Assuming vapor-liquid equilibrium on each stage gives algebraic thermodynamic equations for the relationship between vapor and liquid compositions y_i and x_i. For relatively ideal mixtures, one can often simply assume constant relative volatility, yielding a linear relationship $y_i = \alpha x_i$. Else, if the vapor phase is assumed ideal, the VLE for each component can be described by e.g. Raoult's law together with an activity coefficient model.

3.2 Assumptions and simplifications

The rigorous model presented above is solvable given the relationships for tray hydraulics and VLE. However, a number of simplifications are possible to reduce the model complexity while still capturing the important dynamics of a real column. In the following, step by step, assumptions are made and the resulting simplification to the balance equations are discussed. In the end, we will end up with a simplified, yet sufficiently complex model to use for simulation of a distillation column.

3.2.1 Simplification of energy- and mass balances

(i) *Fixed pressure and neglecting vapor holdup*
A common simplification is to neglect the vapor holdup on each stage ($M_i^v = 0$). When vapor holdup is small compared to liquid holdup, this simplification causes no problems. The assumption may be poor for e.g. high pressure distillation or for volatile components, where the ratio between vapor and liquid holdup becomes larger. Choe and Luyben (1987) recommends including vapor holdup if it exceeds 20% of liquid holdup. Typically it can be neglected for column pressures below 10 bar.

Packed columns usually have low pressure drops. The experimental column is operating at atmospheric pressure, with pressure drop over the column less than 40 mbar. It is therefore reasonable to assume constant pressure equal to 1 bar on all stages.

These assumptions removes the need for a dynamic pressure model, and the mass- and energy balances are simplified slightly; the molar holdup of light component $N_i = M_i^l x_i$, the total holdup $M_i = M_i^l$ and the energy $U_i = M_i^l u_i^l$.

(ii) *Specific energy equal to liquid enthalpy*
After neclecting vapor holdup and assuming constant pressure, we next assume $u^l \approx h^l$ which holds for liquids, such that $U_i = M_i^l h_i^l = M_i h_i^l$. The left side of the

energy balance (3.3) then simplifies to

$$\frac{d}{dt}U_i = \frac{d}{dt}\left(M_i h_i^l\right) = M_i\frac{dh_i^l}{dt} + h_i^l\frac{dM_i}{dt}. \tag{3.6}$$

Combining (3.6) and (3.3) with the overall mass balance (3.2) gives

$$M_i\frac{dh_i^l}{dt} = L_{i+1}(h_{i+1}^l - h_i^l) + V_{i-1}(h_{i-1}^v - h_i^l) + V_i(h_i^l - h_i^v). \tag{3.7}$$

(iii) *Constant and equal liquid enthalpy on all stages*
The model can be further simplified by assuming the liquid enthalpy to be constant, $dh_i^l/dt = 0$, and equal on all stages, $h_i = h_{i+1}$. This assumption is valid as long as the difference in heat capacities for the components is not too big at the relevant pressures. At one bar the molar heat capacity of water is $c_{p,water} \approx 75\frac{J}{molK}$ while methanol has $c_{p,methanol} \approx 80\frac{J}{molK}$, which is close. If the components have a large heat of mixing or if pressure variations are large, one should avoid using the constant enthalpy simplification.

The energy balance with constant enthalpy reduces to an algebraic equation:

$$M_i\frac{dh_i^l}{dt} = 0 = V_{i-1}(h_{i-1}^v - h_i^l) + V_i(h_i^l - h_i^v). \tag{3.8}$$

(iv) *Constant molar vapor flow*
The last simplification to the energy balance is to assume equal heat of vaporization for both components, making $h_i^v = h_{i-1}^v = h^{vap}$. Substituting this into (3.8) and the overall material balance (3.2) gives the popular constant molar vapor flow model

$$V_{i-1} = V_i, \tag{3.9}$$

and the mass balance

$$\frac{d}{dt}M_i = L_{i+1} - L_i. \tag{3.10}$$

In words, the vapor flow up the column is equal on all trays. At steady state the liquid flow $L_i = L_{i+1}$, but dynamically these are not equal since the liquid holdup varies. Equations (3.9) and (3.10) are the simplified energy and overall mass balances. The component mass balance remains unchanged.

3.2.2 Tray hydraulics

As noted previously it is, for feedback control, usually sufficient to assume a linear relationship between stage holdup and internal flows

$$L_i = L_i^{nom} + \lambda(V_i - V_i^{nom}) + \frac{1}{\tau_l}(M_i - M_i^{nom}), \tag{3.11}$$

where τ_l is the hydraulic time constant and superscript *nom* denotes nominal values.

In a packed column one can set $\lambda = 0$ because the initial effect on the liquid flow from a change in vapor flow is usually negligible. The linearized tray hydraulics then becomes

$$L_i = L_i^{nom} + \frac{1}{\tau_l}(M_i - M_i^{nom}). \tag{3.12}$$

The hydraulic time constant $\tau_l \approx \theta_l/N$. Here θ_l is the apparent delay for a step increase in reflux to reach the boiler and N is the number of stages between the boiler and the reflux entrance. M_i^{nom} and τ_l are model parameters and are most easily identified by implementing a step on the reflux flow and fitting the model temperature response to the experimental temperature response.

3.2.3 Thermodynamic equilibrium

Methanol/water does not have a constant relative volatility, therefore more complex thermodynamic relationships are needed. By assuming ideal vapor phase behavior, the relationship between liquid and vapor mole fractions for component $k(= \{1, 2\})$ is modeled by Raolt's law

$$P_k y_k = x_k \gamma_k P_k^{sat}. \tag{3.13}$$

The vapor pressure P_k^{sat} for each component can by found from the Antoine equation

$$\log P_k^{sat} = A_k - \frac{B_k}{T + C_k}, \tag{3.14}$$

and the activity coefficients γ_k are found using Wilson's equation

$$\ln \gamma_k = 1 - \ln\left(\sum_i x_i \Lambda_{ki}\right) - \sum_j \left(\frac{x_j \Lambda_{jk}}{\sum_i x_i \Lambda_{ji}}\right), \tag{3.15}$$

where $i, j = 1, 2$ and

$$\Lambda_{ij} \equiv \frac{V_j}{V_i} \exp\left(\frac{-A_{ij}}{RT}\right). \tag{3.16}$$

The molar volumes V_i, the Wilson parameters A_{ij} and the Antoine equation parameters for a water/methanol mixture are found in chemical data tables (Gmehling and Onken, 1977). Wilson's equation is generally found to represent vapor-liquid equilibrium data very well (Fredenslund et al., 1977).

3.2.4 Effect of feed and reflux conditions

The experimental column has no feed pre-heater, the feed enters at room temperature. Some of the energy within the feed entering stage will therefore be used to heat the feed

to its boiling point. The energy to heat the feed comes from the energy in the rising vapor, and as a consequence a fraction of the rising vapor flow will condense and return as liquid flow down the column from the feed section. Similarly the vapor flow rising up from the feed stage will decrease. To include the effect of cold feed, we first represent the condition of the feed by the quantity q, which is defined as (Geankoplis, 1993)

$$q = \frac{\text{heat needed to vaporize 1 mol of feed at entering conditions}}{\text{molar latent heat of vaporization of feed}} \tag{3.17}$$

If the feed enters at its boiling point, the numerator of (3.17) equals the denominator and $q = 1$. For cold liquid feed $q > 1$, if $q < 1$ it means that some of the feed is already vaporized, while if $q < 0$ the feed is super-heated.

Equation (3.17) can also be written in terms of enthalpies:

$$q = \frac{h_V - h_F}{h_V - h_L}, \tag{3.18}$$

where h_V is the enthalpy of the feed at the dew point, h_L the enthalpy at the boiling point and h_F the enthalpy of the feed at its entrance condition.

The liquid and vapor streams leaving the feed stage NF at steady state becomes

$$L_{NF} = L_{NF+1} + q_F F \tag{3.19}$$
$$V_{NF} = V_{NF-1} + (1 - q_F)F \tag{3.20}$$

Sub-cooling is present at the entrance of the reflux flow as well. The total condenser cools the distillate vapor to liquid with a temperature well its dew point. For the flows leaving the reflux entrance stage $NT - 1$ we get at steady state

$$L_{NT-1} = q_L L_{NT} \tag{3.21}$$
$$V_{NT-1} = V_{NT-2} + (1 - q_L)L_{NT} \tag{3.22}$$

With a entering temperature of 20°C, $q_F \approx 1.1$ and $q_L \approx 1.1$ for the feed and reflux respectively.

3.2.5 Volumetric and molar flow

While it is convenient to use molar flows in the balance equations, it is more natural to use mass- or volumetric flows as inputs to the column since most flow-measurement devices are for mass- or volumetric flows, not molar flows. Also the volumetric feed and reflux flow rates are close to affine in the power input to the pumps.

For a binary mixture the transformation between volumetric reflux, L_q, and molar reflux, L, is given by

$$L_q = LV_{\text{mix}}; \quad V_{\text{mix}} = y_d V_1 + (1 - y_d)V_2, \tag{3.23}$$

where V_1 and V_2 are the molar volumes of the light and heavy components respectively, and y_d is the composition of the reflux.

For the feed flow the transformation is similar, just replace L with F and y_d with z_F, the composition of the feed, in the above equations.

3.2.6 Boiler input

Although feed and reflux is measured on a volumetric basis, the molar vapor flow from the boiler, V, is assumed affine in heating power:

$$h^{vap}V = u_v - Q, \tag{3.24}$$

where h^{vap} is the heat of vaporization for the boiler content, u_v is the power input from the heating coils and Q is the net heat loss from the boiler to the surroundings. The heat of vaporization for the boiler holdup is assumed constant since the boiler composition is nearly constant. The heat loss Q is in addition dependent on boiler holdup and temperature difference between the inside and the outside of the boiler, which is also subject to only small variations. The heat loss is therefore assumed constant. In simulations $h^{vap} = 4.07 \cdot 10^4$kJ/kmol and $Q = 300$W.

3.3 Summary of nonlinear simulation model

The column model consists of overall and component material balances and vapor/liquid phase modeled by Wilson's activity coefficient model. The resulting mathematical model takes the form of a set of differential and algebraic equations (DAE system) with two states for every stage. Below follows a summary of the model assumptions and the resulting equations. The equations for stages with external product streams are written explicitly.

3.3.1 Model assumptions

1. Staged distillation column (numbered from bottom to the top)
2. Perfect mixing and equilibrium in all stages
3. No vapor holdup on stages
4. Liquid flow linear in stage holdup
5. Constant molar vapor flow in column sections
6. Constant pressure in column ($P = 1$ bar)
7. Total condenser
8. VLE calculations from Wilson's equation
9. Consider only normal operation (e.g. no flooding, weeping etc.)

3.3.2 Model equations

Regular stage

$$\frac{d}{dt}M_i = L_{i+1} - L_i + V_{i-1} - V_i \tag{3.25}$$

$$\frac{d}{dt}(M_i x_i) = L_{i+1}x_{i+1} - L_i x_i + V_{i-1}y_{i-1} - V_i y_i \tag{3.26}$$

$$V_i = V_{i-1} \tag{3.27}$$

Condenser $i = NT$

$$\frac{d}{dt}M_i = V_{i-1} - L - D \tag{3.28}$$

$$\frac{d}{dt}(M_i x_i) = V_{i-1}y_{i-1} - Lx_i - Dx_i \tag{3.29}$$

Reflux entrance $i = NT - 1$

$$\frac{d}{dt}M_i = L_{i+1} - L_i + V_{i-1} - V_i \tag{3.30}$$

$$\frac{d}{dt}(M_i x_i) = q_L L_{i+1}x_{i+1} - L_i x_i + V_{i-1}y_{i-1} - V_i y_i \tag{3.31}$$

$$V_i = V_{i-1} + (1 - q_L)L_{i+1} \tag{3.32}$$

Feed stage $i = NF$

$$\frac{d}{dt}M_i = L_{i+1} - L_i + V_{i-1} - V_i + F \tag{3.33}$$

$$\frac{d}{dt}(M_i x_i) = L_{i+1}x_{i+1} - L_i x_i + V_{i-1}y_{i-1} - V_i y_i + F z_F \tag{3.34}$$

$$V_i = V_{i-1} + (1 - q_F)F \tag{3.35}$$

Reboiler $i = 1$

$$\frac{d}{dt}M_i = L_{i+1} - V - B \tag{3.36}$$

$$\frac{d}{dt}(M_i x_i) = L_{i+1}x_{i+1} - V_i y_i - Bx_i \tag{3.37}$$

$$V_i = V \tag{3.38}$$

VLE The algebraic relationship $y_i = f(x_i, T_i)$ between the vapor composition y_i and the liquid composition x_i and stage temperature T_i on all stages are found from Raoult's law and Wilson's equation.

Tray hydraulics The liquid flow deviation is linear in liquid holdup deviation for all trays:

$$L_i = L_i^{nom} + \frac{1}{\tau_l}(M_i - M_i^{nom}). \tag{3.39}$$

3.4 Experimental parameter fitting

3.4.1 Heat loss

The heat loss term Q included in the equation for the vapor flow rate, $h^{vap}V = u_v - Q$, was found by measuring the flow rate with different inputs u_v to the boiler, which was filled with water. The flow rate was measured by letting the vapor rise up the column, with no reflux, and through the condenser. The volume of the condensate was measured over a time interval, and the heat loss calculated from the equation above. Doing this with different input values gave an average heat loss $Q = 300$W, which does not seem unreasonable, considering that the boiler is not insulated.

3.4.2 Number of stages

Earlier experiments have shown that the column has 13 theoretical stages (Reppe, 2004). This was found by driving both the experimental column and the column model to a steady state and match the two temperature profiles. The slope of the model temperature profile can be made more steep or less steep by adjusting the number of theoretical stages, and choosing the number of stages to be 13 gave the best match for the slope.

3.4.3 Nominal holdup and time constant for tray hydraulics

The two remaining key parameters for the system dynamics are the nominal liquid holdup on the stages, M_i^{nom}, and the liquid time constant, τ_l, in the linear tray hydraulics relationship

$$L_i = L_i^{nom} + \frac{1}{\tau_l}(M_i - M_i^{nom})$$

Determining the two parameters is most easily (from a practical point of view) done by recording the initial temperature response to a step change in external reflux (Wittgens, 1999). The hydraulic time constant can be determined from the measurement of the delay θ from a change in external reflux until the liquid outflow of tray N changes;

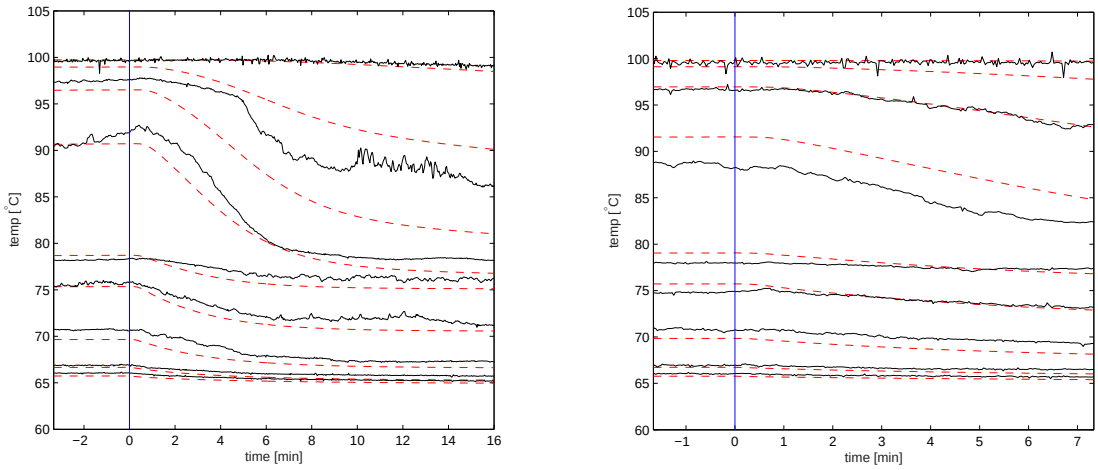

Figure 3.2: Steps in reflux. The figure to the left shows the temperature response to a 5% step increase in reflux rate, the figure to the right shows a similar response to a 10% increase in reflux rate. The solid lines are the measured temperatures along the column, while the dashed lines are selected stage temperature outputs from the model. Model parameters are given in Table 3.1

$\theta = \tau_I N$ (this is an approximation of the effective delay of N first order filters in series; $1/(\tau_I s + 1)^N \approx e^{-\tau_I N s}$). The initial temperature response will indicate the time a reflux change needs to propagate through the column, and increasing τ_l in the model will increase the propagation time.

The holdup on each stage affects the slope of the temperature response, and by adjusting the nominal holdup level it is possible to match the slope of the temperature response in the model with experimental data.

Figure 3.2 shows two comparisons of the experimental and model temperature responses from a step change in reflux, where the model parameters are adjusted to yield a reasonable match. Keep in mind that the temperature measurements in the experimental column is not located on a particular theoretical stage. The model temperature response for a particular stage should have the same shape as the measured temperatures in that region, not necessarily the same absolute value.

Most of the experimental and model temperature responses have similar shapes. One exception is the measured temperature initially at roughly $78°C$. The feed stream is inserted directly above this sensor, which is why the measurement shows less movement than what the model predicts. The temperature measurement starting at 90°C in the left plot is not completely steady initially, which causes a discrepancy between the measured response and the model output. Note also that even though the sensors are located in the same place physically in both of the step responses, it seems like the location relative to the theoretical stages in the model changes. While, for instance, experimental temperature

Table 3.1: Model parameters

Parameter	Boiler	Below feed	Above feed	Condenser
Stage #	1	2-5	6-12	13
τ_l [sec]		46.2	4.8	
M_i^{nom} [mol]	332	0.162	0.772	12.2

number two from the top (starting at 97°C) is located between model temperature two and three for the large step shown in the left plot, it is equal to model temperature three for the smaller step in the right plot. This illustrates that the physical height equivalent of a theoretical stage varies as the composition inside the column changes. In one operating point a temperature measurement may correspond to a given theoretical stage, while if in a different operating point, the measurement may correspond to the neighboring theoretical tray. This is important if one tries to design a temperature based composition estimator based not only on experimental data, but also on the model outputs, as is discussed in chapter 4.

Both the time constant and holdup are chosen equal for all stages above the feed entrance, and equal, but with a different value, below the feed. The holdups in the condenser and boiler were during experiments kept constant at the nominal levels of 0.5 and 6 liters respectively. When calculating the corresponding number of moles, it is assumed pure water in the boiler and pure methanol in the condenser. Parameter values for the simulation model are given in Table 3.1.

Nominal holdup above the feed is approximately 6% of total rectifying section volume, the holdup below the feed is approximately 2% of total stripping section volume. (To calculate the column holdup volume it is assumed an average composition of $x_i = 0.5$ on all stages, the percent values changes somewhat when other composition profiles are used since the molar volume of methanol is roughly twice as big as the molar volume of water.) This is in good correspondence with numbers given by Skogestad (1997), which states that typical holdup for packed columns is about 2.5-5% of the total column volume.

Skogestad further states that τ_l is typically 5 seconds for trayed columns, which is close to the obtained parameter value $\tau_l = 4.8$ seconds, above the feed, in the packed column. Below feed entrance, the time constant is much larger than expected. This is probably because the reflux steps were done from steady state *with feed turned on*. The feed flow generates a pinch region around the feed entrance, which stops interactions between the two column sections.

For both packed and trayed columns the overall liquid lag θ may be estimated from

$$\theta = nM_{tot}/L \tag{3.40}$$

where M_{tot} is the total column holdup, and typically $n = 0.67f$ for trayed columns. Here f is the fraction of liquid holdup above the weir; typically f is about 0.5, but it may be much smaller for small diameter columns. When combining this formula with $\theta = N\tau_l$

and with a nominal reflux flow of $L = 0.97$ mol/min used in the experiments we get, when only considering the rectifying section,

$$f = \frac{\theta L}{0.67 M_{tot}} = \frac{\tau_l L}{0.67 M_i^{nom}} = \frac{4.8/60 \cdot 0.97}{0.67 \cdot 0.772} = 0.15,$$

which is somewhat less then 0.5. This discrepancy may be contributed to the small diameter of the experimental column. When doing the same calculations for the bottom section, we get $f \approx 7$, and summing over the whole column from reflux entrance to above the boiler we get $f \approx 1$. These values of f are not close to the typical value, which again is probably because of the pinch region generated by the feed.

To conclude, the experimental and model temperature responses show similar initial dynamics and the values of the parameters obtained correlates well with the typical values given by Skogestad when considering the section above the feed entrance. Below the feed, there is basically no correspondence, mainly because the temperature responses where recorded from a steady state with a pinch zone around the feed.

4. Composition estimator

It can be difficult to obtain reliable and accurate measurements of product compositions for distillation column control. Accurate measurements from e.g. a gas chromatograph have measurement delays of several minutes or more. Other possible measurement devices like infrared, ultraviolet or refractive index analyzers have shorter time delay, but may need frequent calibration.

Temperature is frequently used instead of online composition measurement. Measuring temperature is easy, and is both fast and reliable. The challenge is then to find a relation between measured temperatures and product compositions, i.e. a composition estimator. Product composition estimators based on temperature measurements have been constructed in several ways, and Mejdell (1990) compares some of them. We will here use a static linear estimator with logarithmical inputs and outputs, which gave good results in Mejdell's comparison.

4.1 Problem definition

The following problem is treated: Given temperature measurements at several locations within the distillation column, find a good static estimator of the product compositions. The column considered has seven temperature sensors and separates a binary mixture of methanol and water.

4.1.1 The estimation problem

Consider the case with binary mixture and constant pressure. The steady state temperature profile in the column is uniquely determined from the values of the feed composition z_F, distillate composition y_d, and bottoms composition x_b as

$$\theta = f(z_F, y_d, x_b), \tag{4.1}$$

where θ is the temperature profile. We want to find the inverse relation to get the estimates

$$\hat{y} = \begin{pmatrix} \hat{y}_d \\ \hat{x}_b \end{pmatrix} = g(\theta^{7\times 1}), \tag{4.2}$$

where g is a nonlinear function of the 7 measurements of the temperature profile, $\theta^{7\times 1}$.

4.1.2 Transformed variables

The composition and temperature profiles are nonlinear functions of the operating variables. Logarithmic transformations are known to capture these nonlinearities and to linearize the dynamic and static responses (see e.g. Skogestad and Morari, 1988). For binary mixtures the distillate and bottoms composition transformations are

$$Y_d = \ln(1 - y_d); \quad X_b = \ln(x_b). \tag{4.3}$$

The temperature profile may also be linearized using a similar transformation:

$$L_T = \ln\left(\frac{\theta - T_L^b}{T_H^b - \theta}\right). \tag{4.4}$$

Here T_L^b and T_H^b are the boiling temperatures of the light and the heavy components respectively. This transformation results in a nearly linear column profile, except from possibly a pinch zone around the feed.

Day-to-day and during operation pressure variations will change the boiling temperatures T_L^b and T_H^b. Therefore, instead of using boiling temperatures in the transformation, we use the implicitly pressure compensated transformation

$$L_\theta = \ln\left(\frac{\theta - \theta_L}{\theta_H - \theta}\right). \tag{4.5}$$

The boiling temperatures are replaced with reference temperatures θ_L and θ_B selected at the column ends, which is close to the boiling temperature of the pure components regardless of pressure variations.

4.1.3 Linearized composition estimator

With logarithmical input temperatures and output compositions, the remaining part of the estimator g in (4.2) is assumed locally linear

$$\Delta\hat{Y} = \begin{pmatrix} \Delta\hat{Y}_d \\ \Delta\hat{X}_b \end{pmatrix} = K\Delta L_\theta, \tag{4.6}$$

where the Δ's denote deviation variables. A calibration set with several parallels of measured compositions and temperatures is used to find a suitable estimator K.

Because temperatures close to each other changes in nearly the same way, the temperature data is likely to be collinear. A general least squares solution for finding K will because of the collinearity be badly conditioned, and hence sensitive to temperature noise. To avoid the problem of dependent input variables, a better approach is to use partial least squares (PLS) regression. In PLS regression a linear input projection is used

to select directions in the input variables which have large covariance with the output variables. The projected inputs are called the latent variables, spanned by linear combinations of the temperatures. The latent variables are used as new estimator inputs and are constructed to explain as much as possible of the *output* variation. (A different and well known method, principal component regression, on the contrary selects the main directions of the input variables, the principal components, as latent variables, thereby covering as much as possible of the *input* variations.) The latent variables should preferably be independent and contain all the original information relevant for estimating the compositions. The reader is referred to Naes and Martens (1985) and de Jong (1993) for more details on prediction and PLS-regression.

4.2 Calibration set

To obtain a calibration set for the estimator, the distillate and bottoms from the experimental column were sampled under different operating conditions (varying L, V, F and z_F). The samples were analyzed by Statoil in their lab at Tjeldbergodden.

Data was collected from a total of 22 parallels. It turned out that 12 of the parallels were too far away from the desired operating region, and were therefore not used. The thrown-away parallels were pure in one of the products, while the other product would be impure, e.g. $x_b = 0.001$ and $y_d = 0.7$. It was not possible, nor desirable, to get a good fit to these parallels, and they were deleted from the calibration set.

The first parallels were done by manually adjusting the inputs and then let the column settle to a steady state before product samples were taken. This was time consuming — it takes hours for the open-loop column to settle. Therefore two proportional controllers were added, between a temperature in the upper half of the column and the reflux flow, and between a temperature in the lower part and the vapor flow. The P-controllers made the column reach steady state faster, and hence made it possible to take product samples more frequently. The controllers also made it easier to make sure the steady-state temperature profiles ended up reasonably close to a nominal operating point.

The temperature profiles used in the calibration set are shown in Figure 4.1, and are the average of the measured temperatures at the sample time plus minus five minutes.

After an estimator had been created and used on the experimental column for a few weeks, temperature sensor number 5 broke down and started to show a temperature of 850°C, in other words a broken circuit. Because of a somewhat unfortunate sensor placement design, replacing the sensor can not be done without dismounting the top column section and remove the packing. This will alter the position of the remaining sensors in the top section, and a new set of calibration data may be needed if the sensor positions change significantly. Instead a new estimator was calculated using only the seven remaining sensible temperature measurements, disregarding the broken one.

The column was not equipped with many temperature measurements in the first place,

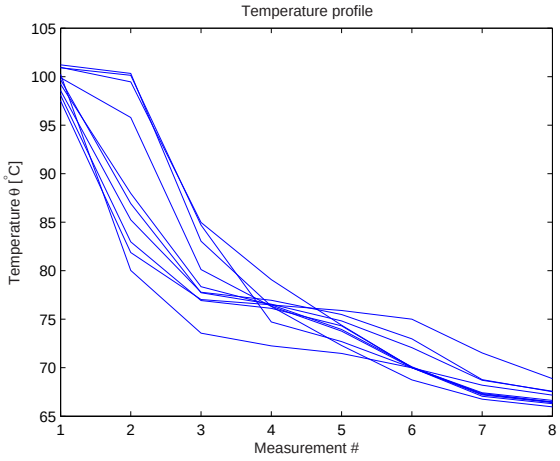

Figure 4.1: Temperature profiles for the parallels in the calibration set. Feed enters at measurement # 4.

and removing one turned out to make a significant difference for the estimator quality. Initially both the bottoms and the distillate composition estimates were dependent on all measured temperatures. With eight sensors, the bottoms estimator gave more weight to temperatures below the feed and the distillate composition estimator gave more weight to temperatures high up in the column. With only seven temperatures, this separation disappeared and suddenly the bottoms estimator became highly dependent on temperatures above the feed and the distillate estimator dependent on temperatures close to the boiler. This is both un-physical and makes control harder because of an increased time delay between internal flow changes and valid composition estimates.

To remove the dependency on temperatures far away, a new bottoms estimator was calculated using only temperatures 1 to 4 in the calibration data and a new distillate estimator was calculated using temperatures 6, 7 and 8. Temperatures 1 and 8 were still used as reference temperatures in the temperature transformations.

The logarithmical calibration data was centered and scaled before used in the PLS regression. Mejdell's proposed scaling method was used, where not only data variance, but also residuals between the original calibration data and the latent variables are accounted for: $W_i = (\sigma_{ci} - \sigma_{e_k i})/\sigma_{ci}^2$. Here σ_{ci} is the standard deviation of temperature i in the calibration set, and $\sigma_{e_k i}$ is an estimate of the additional noise error introduced by projecting the temperature variables onto latent variables. When there is no noise ($\sigma_{e_k i} = 0$) this weight scales the variables to unit variance, and if all variation is unexplained ($\sigma_{e_k i} = \sigma_{ci}$), measurement i is given zero weight. This scaling slightly improved the initial design where K was calculated as a full 2×8 matrix with all temperatures available, and provided for a better estimator than when ignoring noise error in the scaling. With fewer temperature measurements it made no difference, since the latent variables then basically spanned the entire input temperature space.

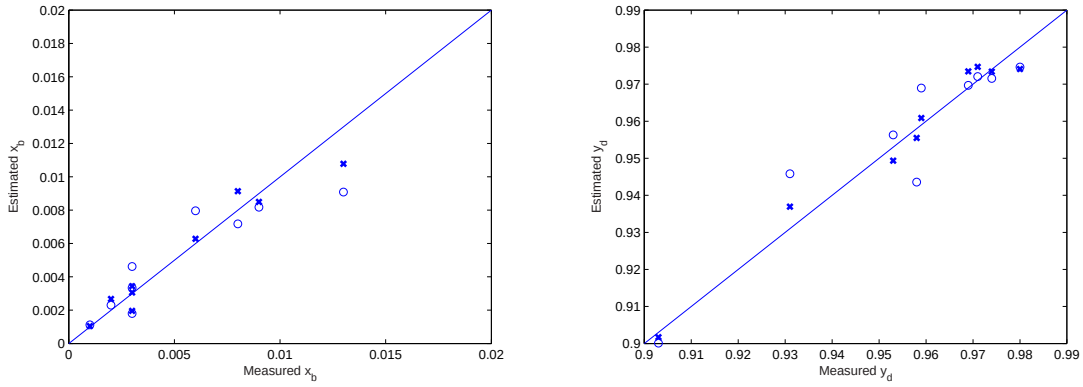

(a) Bottom product

(b) Top product

Figure 4.2: Composition estimates. Circles: estimator with nearby temperatures; x-mark: estimator with all 8 temperatures.

4.3 Results and discussion

Three latent variables were used when calculating the estimator with eight temperature inputs. Increasing the number of latent variables gives a better fit to the calibration data, but at the risk of over-parameterizing and becoming too sensitive to temperature variations. Since the column itself has only three degrees of freedom, three factors would account for 100% of the variance if the column was linear, which the linearizing transformations help to achieve. The three main factors are due to changes in external streams, changes in internal streams, and changes in feed composition, which all affect the temperature profile in distinct ways. When using a reduced number of temperatures, the PLS regression becomes similar to ordinary least squares. The number of latent variables then equals the number of temperature measurements, and the input projection does not change the data in any way.

The N-way toolbox[1] contains an implementation of the PLS regression algorithm and was used when calculating the estimator. Figure 4.2 shows how the estimates correlates with the actual compositions for the estimators calculated with all temperatures available and when using only nearby temperatures. The straight lines indicate perfect correlation. The top product compositions cover a wide range from $y_d = 0.9$ to $y_d = 0.98$, while the bottom product compositions on the other hand cover a narrower region. With full temperature information (marked x in figure), the estimates generally fits well to the actual compositions, but still some estimates seem to suffer from too few temperature measurements to capture the temperature profile. Four parallels, with distillate compositions ranging from $y_d = 0.97$ to $y_d = 0.98$, basically give the same estimated value $\hat{y}_d = 0.97$, and three parallels with $x_b = 0.003$ have estimates varying from $\hat{x}_b = 0.002$ to $\hat{x}_b = 0.004$.

[1] `http://www.models.kvl.dk/source/nwaytoolbox/index.asp`

Especially the distillate estimator yields larger errors with fewer temperature measurements (marked o in figure). The failing sensor was in the top section, and removing this sensor hides vital information from the top composition estimator.

Originally there where several parallels with less pure bottoms compositions available which could have been used to extend the bottoms range, however they were difficult to include in the calibration set. All the bottoms composition estimates $\hat{x}_b$ became markedly worse when parallels with less pure bottoms were included. The top product estimator was not as sensitive to adding parallels. A reason may be that most of the temperature variation in the calibration set is below the feed, and that most of the separation is done in the bottom section. The pinch region generated by the feed may also to a higher extent affect the bottoms estimator. Mejdell (1990) did also report a less accurate bottoms estimator.

It is not possible to say much more on the quality of the estimator without cross-validating the estimator with experiments not used in the calibration set. With few parallels available it is not desirable to divide the data into one calibration set and one cross-validating set; all the parallels are needed in the calibration to obtain a reasonable estimator. More data should be collected to improve the estimator and allow for cross-validating. A few samples were taken during column operation and analyzed using a pycnometer. Even though not accurate enough to be used as calibration or validation data, the distillate samples were all purer than the estimates said. The bottoms samples were all pure, both according to pycnometer tests and according to the estimates.

One may question using a static composition estimator instead of a dynamic estimator. The reason why a static estimator can be made to work, is that the compositions and the temperatures have similar dynamic responses, even more so when only using temperature measurements close to the product composition being estimated.

Collecting calibration data is a tedious and time consuming process. It would definitely be nice if one could use a model based estimator, e.g. simply use the temperature and composition outputs from a dynamic column model in addition to experimental data for the calibration described above. This turned out to be more difficult than first expected. The main problem was that even though the shape of the model and experimental dynamic temperature response could be made similar, it was not possible to consistently fit the values of the actual temperature outputs to the model temperature outputs. The model has 13 temperature outputs, one on each theoretical stage, while the actual column has seven temperature measurements, each located somewhere between two neighboring "stages". When exciting a column input, a particular measured temperature θ_i would appear to be located somewhere between two theoretical stages in the corresponding model output. These two model temperature outputs were then combined linearly to fit to θ_i, which yielded a seemingly accurate model temperature for that particular step. However, when doing a different input step to cross-validate, θ_i could be located between two different model stages, and the linearly combined model temperatures would be too far away from the actual temperature to be used for calibration data in a composition estimator.

5. H_∞ loop shaping theory

So far we have looked at how to model the distillation system without explicitly considering uncertainty. It is not possible, nor even desirable, for a mathematical model to capture everything affecting the system dynamics. It is not possible because we do not know everything, it is not desirable because such a model would generally be far too complex for our purposes. There are other reasons as well, the point is that there will always be a mismatch between the real system and the system model — model uncertainty.

In robust control, explicit consideration is taken to make sure that the closed-loop system is satisfyingly controlled even in the presence of uncertainty. H_∞ is a method used in robust control theory for designing controllers, where mathematical restrictions are made on the size of transfer functions in the H_∞ norm sense. The H_∞ system norm is the maximum amplification a system can make to the energy of its input signal. In the MIMO case, it is equal to the system's maximum singular value over all frequencies, reducing to the maximum value of the frequency response magnitude in the SISO case.

To elaborate on typical H_∞ analysis and synthesis problems, consider the general system shown in Figure 5.1. Here P is the interconnection matrix, K is the controller, Δ is the set of all possible uncertainties, w is a vector signal including noises, disturbances and reference signals, z is a vector signal including all controlled signals and tracking errors, u is the control signal and y is the measurement. Let T_{zw} be the transfer function

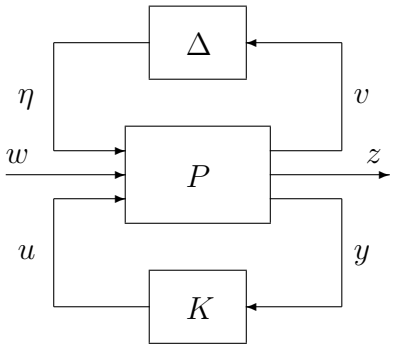

Figure 5.1: General control configuration

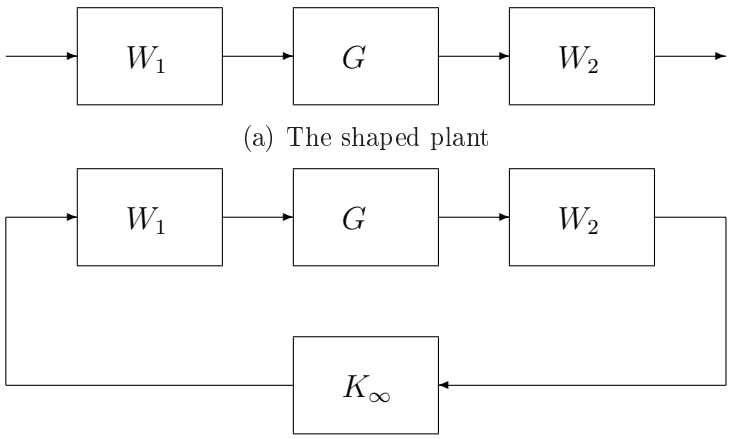

(a) The shaped plant

(b) H_∞ compensation

Figure 5.2: The loop shaping design procedure

from w to z, and assume that the uncertainty Δ satisfies $\|\Delta\|_\infty \leq 1/\gamma_u$. The analysis problem is then to answer if the closed-loop system is stable for all admissible Δ, and if the H_∞ norm of T_{zw}, $\|T_{zw}\|_\infty \leq 1/\gamma_p$ for some prespecified γ_p. The synthesis problem is to design a controller K so that these robust stability and performance conditions are met. For more on different H_∞ problem formulations, see e.g. Skogestad and Postlethwaite (1996) or Zhou and Doyle (1998).

H_∞ loop shaping is, due to its simplicity, an appealing H_∞ controller design method proposed in the late eighties (see Glover and McFarlane, 1989; McFarlane and Glover, 1990). It differs from conventional H_∞ design methods in that no uncertainty model is required prior to the controller synthesis. Instead the controller is designed to maximize the set of admissible uncertainties. The H_∞ loop shaping design procedure consists of two steps, as illustrated in Figure 5.2:

1. *Loop shaping*: A desired open-loop shape is obtained by adding pre- and post-compensators to the nominal plant model. The nominal plant, G, and shaping functions, W_1 and W_2, are combined to form a shaped plant, G_s, where $G_s = W_2GW_1$ (see Figure 5.2(a)). This step is used to obtain a desired level of performance.

2. *Robust stabilization*: The shaped plant G_s is robustly stabilized with respect to coprime factor uncertainties using H_∞ robust stabilization (see Figure 5.2(b)). This step maximizes the admissible uncertainty set.

In the following we take a look at these two steps individually.

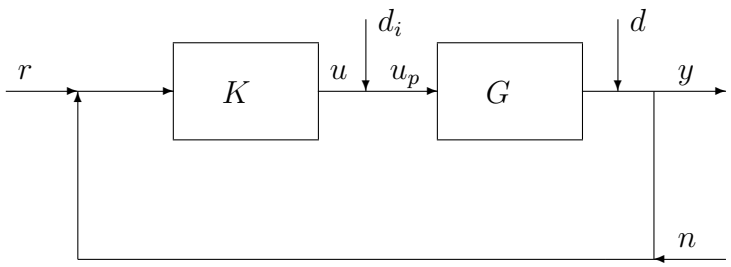

Figure 5.3: Closed loop system

5.1 Loop shaping

Robust stabilization *alone* is not much use in practice because the designer is not able to specify any performance requirements. McFarlane and Glover (1990) add pre- and post-compensators to the nominal plant to shape the singular values of the compensated subsystem, and thereby achieves a way of affecting the closed loop performance. The idea of loop shaping is that the singular values of particular closed-loop transfer functions can be determined by looking at the corresponding open-loop transfer functions, and these singular values are physically meaningful. The classical paper by Doyle and Stein (1981) gives a comprehensive introduction to multivariable loop shaping methods, and it is now discussed in most textbooks on robust control (see e.g. Green and Limebeer, 1995; Zhou and Doyle, 1998).

5.1.1 What is a desired loop shape?

To discuss the idea of loop shaping, consider the feedback system in Figure 5.3. For convenience define the *input loop transfer function*, L_i, and the *output loop transfer function*, L_o, as

$$L_i = KG, \quad L_o = GK. \tag{5.1}$$

L_i is obtained by breaking the loop at the plant input u, while L_o is obtained by breaking the loop at the plant output y. The *input sensitivity* matrix is defined as the transfer function matrix from d_i to u_p:

$$S_i = (I - L_i)^{-1}; \quad u_p = S_i d_i. \tag{5.2}$$

The *output sensitivity* matrix is defined as the transfer function matrix from d to y:

$$S_o = (I - L_o)^{-1}; \quad y = S_o d. \tag{5.3}$$

The *input* and *output complementary sensitivity* matrices are defined as

$$T_i = I - S_i = L_i(I - L_i)^{-1}, \tag{5.4}$$

$$T_o = I - S_o = L_o(I - L_o)^{-1} \tag{5.5}$$

respectively.

Some calculations give the following equations for the closed loop system:

$$y = T_o(r+n) + S_oGd_i + S_od, \tag{5.6}$$
$$r - y = S_o(r-d) - T_on - S_oGd_i, \tag{5.7}$$
$$u = KS_o(r+n+d) + T_id_i, \tag{5.8}$$
$$u_p = KS_o(r+n+d) + S_id_i. \tag{5.9}$$

These equations reveal different design objectives. Good disturbance rejection at the plant output (y) and small tracking error ($r-y$) requires the output sensitivity transfer matrix S_o and also S_oG to be small in the frequency range where d and d_i are large respectively (typically at low frequencies). Good disturbance rejection at the plant input (u_p) requires the input sensitivity transfer matrix S_i to be small where d_i is large and KS_o small where d is large (also typically at low frequencies).

These objectives can be transformed into objectives on the open-loop transfer functions. Making the input and output sensitivities small in terms of singular values is equivalent to making the loop gains large because

$$\underline{\sigma}(L_i) \gg 1 \Leftrightarrow \bar{\sigma}(S_i) = \bar{\sigma}((I-L_i)^{-1}) = 1/\underline{\sigma}(I-L_i) \leq 1/(\underline{\sigma}(L_i)-1) \ll 1, \tag{5.10}$$
$$\underline{\sigma}(L_o) \gg 1 \Leftrightarrow \bar{\sigma}(S_o) = \bar{\sigma}((I-L_o)^{-1}) = 1/\underline{\sigma}(I-L_o) \leq 1/(\underline{\sigma}(L_o)-1) \ll 1. \tag{5.11}$$

Suppose further that G and K are invertible. Then (remember that $L_i = KG$ and $L_o = GK$)

$$\underline{\sigma}(L_i) \gg 1 \text{ or } \underline{\sigma}(L_o) \gg 1 \Leftrightarrow \bar{\sigma}(S_oG) = \bar{\sigma}((I-GK)^{-1}G) \approx \bar{\sigma}(K^{-1}) = 1/\underline{\sigma}(K), \tag{5.12}$$
$$\underline{\sigma}(L_i) \gg 1 \text{ or } \underline{\sigma}(L_o) \gg 1 \Leftrightarrow \bar{\sigma}(KS_o) = \bar{\sigma}(K(I-GK)^{-1}) \approx \bar{\sigma}(G^{-1}) = 1/\underline{\sigma}(G). \tag{5.13}$$

Hence good disturbance rejection at plant output requires large output loop gain, $\underline{\sigma}(L_o) \gg 1$, in the frequency range where d is significant, and large enough controller gain, $\underline{\sigma}(K) \gg 1$, in the frequency range where d_i is significant. Similarly, good performance at plant input u_p requires large input loop gain, $\underline{\sigma}(L_i) \gg 1$, in the frequency range where d_i is significant and large enough plant gain, $\underline{\sigma}(G) \gg 1$, (which cannot be changed by controller design) in the frequency range where d is significant.

By making the sensitivity matrix S_o small we are at the same time making the complementary sensitivity T_o large because $S_o + T_o = I$. In effect, the output becomes more sensitive to measurement noise, n, when the effect of disturbances are desensitized. Typically measurement noise is at high frequency, while disturbances are at low frequency, making it possible to have both disturbance- and noise rejection by designing S_o small at low frequency and T_o small at high frequency.

Another tradeoff concerns command and disturbance error reduction versus stability under model uncertainty. Assume the nominal model G is perturbed via a multiplicative

output uncertainty to $(I + \Delta)G$ with Δ stable, and assume that the nominal ($\Delta = 0$) closed-loop system is stable. The perturbed closed-loop system is stable if

$$\begin{aligned}\det(I - (I + \Delta)L_o) &= \det((I - \Delta L_o(I - L_o)^{-1})(I - L_o)) \\ &= \det(I - \Delta T_o)\det(I - L_o)\end{aligned}$$

has no right-half plane zero. This also requires T_o to be small at frequencies where Δ is significant, typically at high frequencies. T_o is small when the loop gain is small because

$$\bar{\sigma}(L_o) \ll 1 \Leftrightarrow \bar{\sigma}(T_o) = \bar{\sigma}(L_o(I - L_o)^{-1}) \approx \bar{\sigma}(L_o). \tag{5.14}$$

Another issue is that large loop gain outside the bandwidth of G (i.e. L_o or L_i large at high frequency) can make the control activity quite unacceptable. If we assume G to be square and invertible and large loop gain, this follows from (5.8):

$$\begin{aligned}u &= KS_o(r + n + d) + T_i d_i \\ &= K(I - GK)^{-1}(r + n + d) + KG(I - KG)^{-1}d_i \\ &\approx G^{-1}(r + n + d) + d_i \text{ when } \underline{\sigma}(L_i), \underline{\sigma}(L_o) \gg 1.\end{aligned} \tag{5.15}$$

Because $\underline{\sigma}(G^{-1}) = 1/\bar{\sigma}(G) \gg 1$ at frequencies above the bandwidth of G, disturbance and noise is amplified at u when the loop bandwidth significantly exceeds that of G. In other words, it is not possible to make the closed-loop system significantly faster than the open-loop system by increasing the control gain without at the same making the actuators more affected by noise and disturbances.

To summarize, we note that to get good disturbance rejection and tracking requires in some frequency range, typically some low frequency range $(0, \omega_L)$,

$$\underline{\sigma}(L_i) \gg 1 \quad \underline{\sigma}(L_o) \gg 1 \quad \underline{\sigma}(K) \gg 1.$$

Robust stability and sensor noise rejection require in some frequency range, typically some high-frequency range (ω_U, ∞),

$$\bar{\sigma}(L_i) \ll 1 \quad \bar{\sigma}(L_o) \ll 1 \quad \bar{\sigma}(K) \leq M,$$

where M is not too large.

Figure 5.4 indicates graphically how the requirements on these closed-loop objectives constrain the shape of the open-loop singular values. The designer must choose K such that the maximum and minimum singular values of L_i and L_o avoids the shaded regions. In addition, it may be necessary to further adjust $\underline{\sigma}(K)$ over $(0, \omega_L)$ and $\bar{\sigma}(K)$ over (ω_U, ∞).

The singular value shaping seems like a simple approach to design. However, shaping of the open-loop system does not guarantee that the closed-loop system will be internally stable — which cannot be determined from the open-loop singular values. In the SISO

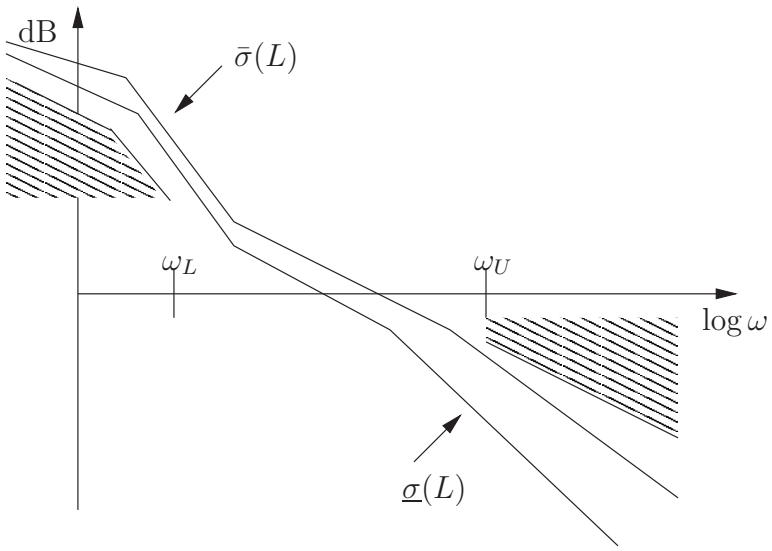

Figure 5.4: Open-loop singular value shaping

case, it is well known that the phase at gain crossover in practical designs cannot exceed 180°, or equivalently, the roll-off rate should be less than 40 db/decade. In the MIMO case there is a similar limitation on the roll-off of the magnitude of the *eigenvalues* of the loop gain (not the *singular values*) in the crossover region. The loop shaping gets involved in the MIMO case because of this additional stability requirement. The designer has to manipulate $\underline{\sigma}(L)$ and $\bar{\sigma}(L)$ to get the desired loop-shape, while at the same time restricting the roll-off rate of the eigenvalues of L to ensure closed-loop stability.

In section 5.2 a technique is presented to deal with the stability issue. First the designer specifies a desired loop shape, using pre- and post-compensators, while ignoring closed-loop stability. Then this shaped plant is robustly stabilized using an additional controller, K_∞, in the feedback path as illustrated in Figure 5.2. This last step will guarantee a certain level of robust stability of the closed-loop system.

Before proceeding to the stabilization step, a particulary simple method for obtaining reasonably well shaped loops is presented.

5.1.2 Loop shaping using PI-controllers

Designing pre- and post-compensators to get a desired loop-shape typically involves several iterations of trial and error, especially for the unskilled designer. A simpler method than jumping directly to the selection of poles and zeros in the transfer functions within the compensators, is to use PI(D)-controllers as the diagonal elements of the pre-compensator. Generally speaking, selecting the PI-controller gains may be just as difficult as selecting a filter directly, but if equipped with a set of descent tuning rules for the PI-controller

gains, this is a straightforward way of obtaining reasonable loop shapes.

Normally the designer of the compensators would as a starting point chose a constant post-compensator and a diagonal pre-compensator consisting of first- or second-order transfer functions. This is also what one will get if using PI- or PID-controllers. With the SIMC tuning guidelines given next, the designer easily obtains a first trial for a compensator, which may be used directly or as a stepping stone to more refined compensators. The compensated plant is then robustly stabilized using H_∞ theory. Of course one can also look at it the opposite way, H_∞ is applied to robustify an already existing PID-controller design.

SIMC-PID tuning rules

Skogestad (2004) presents a set of tuning rules for the PID controller which are both easy to use and work well on a wide range of processes. The procedure for selecting controller gains consists of two steps. Firstly, a first- or second-order plus delay model i obtained. Secondly, controller settings are derived based on the model parameters. PI-setting result from a first-order model, whereas PID-setting result from a second-order model.

Given a process model

$$g(s) = \frac{k}{(\tau_1 s + 1)(\tau_2 s + 1)} \mathrm{e}^{-\theta s}, \tag{5.16}$$

the recommended SIMC-PID settings for the controller

$$c(s) = K_c \left(\frac{\tau_I s + 1}{\tau_I s} \right) (\tau_D s + 1) \tag{5.17}$$

are

$$K_c = \frac{1}{k} \frac{\tau_1}{\tau_c + \theta} \tag{5.18}$$

$$\tau_I = \min\{\tau_1,\ 4(\tau_c + \theta)\} \tag{5.19}$$

$$\tau_D = \tau_2. \tag{5.20}$$

The only tuning parameter is τ_c, and a good starting point is to select $\tau_c = \theta$, the effective delay. A smaller value for τ_c yields a more aggressive controller with better tracking and disturbance attenuation, but at the same time a controller more sensitive to noise. From the equations it is clear that a first-order model ($\tau_2 = 0$) will result in a PI-controller, whilst a second order model will result in a PID-controller.

In his paper, Skogestad also gives guidelines for how to reduce a higher-order transfer function model into a first- or second-order model with dead-time in an easy way, the first step for obtaining controller tunings. This is not pursued any further here.

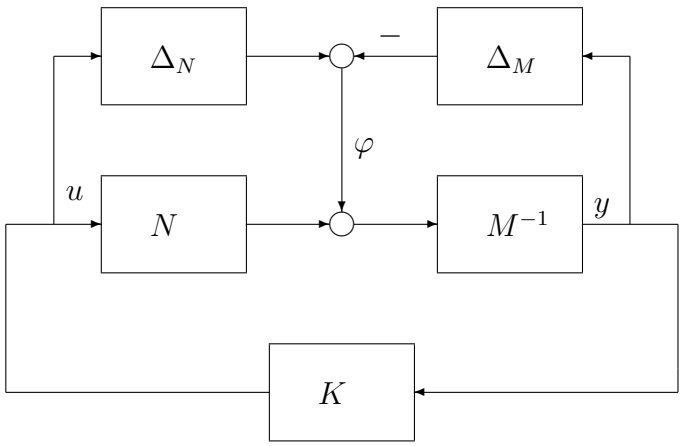

Figure 5.5: Coprime factor robust stabilization problem

5.2 Robust stabilization

In this section a method is presented for robust stabilization of a system with a coprime factor uncertainty description, as illustrated in Figure 5.5. The method was first introduced by Glover and McFarlane (1989).

We are considering perturbations to the normalized left coprime factors of a nominal plant, the shaped plant from the previous section, and find the stabilizing controller which allow the H_∞ norm of the coprime factor perturbations to be as large as possible while maintaining internal stability. This robust stabilization problem has a simple analytical solution, not requiring any γ-iteration.

A normalized left coprime factorization of a nominal plant G is a left coprime factorization $(N,\, M)$ of G such that $G = M^{-1}N$ which satisfies

$$MM^* + NN^* = I \quad \forall s \in j\Re, \tag{5.21}$$

or equivalently, $[N, M]$ is co-inner.

We want to find a particular controller that stabilizes the perturbed plant model

$$G_\Delta = (M + \Delta_M)^{-1}(N + \Delta_N) \tag{5.22}$$

for the largest possible ball of uncertainty $\|[\Delta_N\ \Delta_M]\|_\infty < \epsilon = \gamma^{-1}$. The following theorem gives necessary and sufficient conditions for the closed-loop stability of G_Δ.

Theorem 5.1. *Given the perturbed plant model*

$$G_\Delta = (M + \Delta_M)^{-1}(N + \Delta_N)$$

with M, N, Δ_M and Δ_N stable rational transfer functions. (M, N) is a stable left coprime factorization of G, and K internally stabilizes the nominal system G. Define

$\Delta := [\Delta_N \ \Delta_M]$. *Then the closed loop system shown in Figure 5.5 is internally stable for all* $\|\Delta\|_\infty < \epsilon = 1/\gamma$ *if and only if*

$$\left\| \begin{bmatrix} K \\ I \end{bmatrix} (I - GK)^{-1} M^{-1} \right\|_\infty \leq \gamma$$

Proof. ($\Leftrightarrow$) From visual inspection of Figure 5.5 we see that

$$\begin{bmatrix} u \\ y \end{bmatrix} = \begin{bmatrix} K \\ I \end{bmatrix} (I - GK)^{-1} M^{-1} \varphi$$

$$\varphi = \begin{bmatrix} \Delta_N & -\Delta_M \end{bmatrix} \begin{bmatrix} u \\ y \end{bmatrix}$$

The uncertainty is bounded by $\|\begin{bmatrix} \Delta_N & -\Delta_M \end{bmatrix}\|_\infty = \|\Delta\|_\infty < 1/\gamma$. According to the small gain theorem, the closed loop system is internally stable for all admissible Δ if and only if the loop gain is less than one, which is satisfied if and only if

$$\left\| \begin{bmatrix} K \\ I \end{bmatrix} (I - GK)^{-1} M^{-1} \right\|_\infty \leq \gamma$$

which completes the proof. □

Glover and McFarlane (1989) show that the minimum γ (largest ϵ) such that a single fixed controller K stabilizes the perturbed plant G_Δ for all $\|\Delta\|_\infty < 1/\gamma$ is given explicitly by

$$\gamma_{min} = (1 + \lambda_{max}(XY))^{1/2} \tag{5.23}$$

Given a minimal realization of the plant $G \stackrel{s}{=} (A,\ B,\ C,\ D)$, X and Y are the unique positive definite solutions to the *Control Algebraic Riccati Equation* and the *Filtering Algebraic Riccati Equation*

$$(A - BS^{-1}D^*C)^*X + X(A - BS^{-1}D^*C) - XBS^{-1}B^*X + C^*R^{-1}C = 0 \tag{5.24}$$

$$(A - BS^{-1}D^*C)Y + Y(A - BS^{-1}D^*C)^* - YC^*R^{-1}CY + BS^{-1}B^* = 0 \tag{5.25}$$

where $S \triangleq I + D^*D$ and $R \triangleq I + DD^*$.

A particular controller, referred to as the *central* or *maximum entropy* controller, guaranteeing that

$$\left\| \begin{bmatrix} K \\ I \end{bmatrix} (I - GK)^{-1} M^{-1} \right\|_\infty \leq \gamma \tag{5.26}$$

for a selected tolerance level $\gamma > \gamma_{min}$, is given by the state space realization

$$K \stackrel{s}{=} \left[\begin{array}{c|c} A + BF + \gamma^2 Q^{*-1} Z C^* (C + DF) & \gamma^2 Q^{*-1} Z C^* \\ \hline B^*X & {}^-D^* \end{array}\right] \tag{5.27}$$

$$F = -S^{-1}(D^*C + B^*X) \tag{5.28}$$

$$Q = (1 - \gamma^2)I + XZ \tag{5.29}$$

Remark 5.1. *Note that if $\gamma = \gamma_{min}$, then Q becomes singular ($Q = XZ - \lambda_{max}(XZ)$ is singular) and the controller K as given above cannot be implemented. The truly optimal controller can still be constructed using a descriptor system approach (see Safonov et al., 1989). For $\gamma > \gamma_{min}$, K is sometimes referred to as a sub-optimal controller.*

Remark 5.2. *The two-block problem considered for robust stability above is equivalent to a four-block problem; using the fact that $[N\ M]$ is normalized and co-inner, and since the norm is invariant under right multiplication by a co-inner function, we have*

$$\begin{aligned} &\left\| \begin{bmatrix} K \\ I \end{bmatrix} (I - GK)^{-1} M^{-1} \right\|_\infty \leq \gamma \\ \Leftrightarrow &\left\| \begin{bmatrix} K \\ I \end{bmatrix} (I - GK)^{-1} M^{-1} \begin{bmatrix} N & M \end{bmatrix} \right\|_\infty \leq \gamma \\ \Leftrightarrow &\left\| \begin{bmatrix} K \\ I \end{bmatrix} (I - GK)^{-1} \begin{bmatrix} G & I \end{bmatrix} \right\|_\infty \leq \gamma \end{aligned}$$

Hence, the controller minimizing γ is also the controller minimizing a combination of the closed-loop transfer functions $K(I - GK)^{-1}G$, $K(I - GK)^{-1}$, $(I - GK)^{-1}$, and $(I - GK)^{-1}G$. In the previous section it was shown that $(I - GK)^{-1}$ and $(I - GK)^{-1}G$ are typically used as performance objectives to be kept small at low frequency, while $K(I - GK)^{-1}$ and $K(I - GK)^{-1}G$ reflect robust stability and noise attenuation properties and should be small at high frequency. A more effective design is one in which these transfer function objectives are frequency weighted to trade-off between performance and robust stability over different frequency ranges. This is exactly what is achieved by robustly stabilizing the shaped *plant $G_s = W_2 G W_1$.*

Remark 5.3. *The controller given above is only one out of a set of stabilizing controllers which achieves* (5.26)*. The parametrization of* all *stabilizing controllers is possible, both for $\gamma = \gamma_{min}$ and $\gamma > \gamma_{min}$, using a Nehari extension. This is shown in McFarlane and Glover (1990).*

Remark 5.4. *The H_∞ loop shaping technique uses a normalized coprime factor uncertainty description. This type of model perturbations is known to represent a wide range of uncertainties, e.g. low frequency parameter errors, neglected high frequency dynamics and uncertain right half plane poles and zeros (Zhou and Doyle, 1998).*

We have now established the state-space solution to a particular controller achieving a level ϵ of robustness to model uncertainty. In the previous section we looked at how to set up the problem by using compensators to get a desired loop-shape. In the next section some guidelines will be given for these two design steps, and for how to implement the final controller.

5.3 Design guidelines

As a summary of the H_∞ loop shaping controller design the following guidelines are given, mainly based on guidelines in Skogestad and Postlethwaite (1996):

1. Scale the plant inputs and outputs to enable meaningful analysis and improve conditioning.

2. Make the system as diagonal as possible by ordering inputs and outputs. This makes the design of pre- and post compensators easier, they can frequently be chosen to be diagonal.

3. Select the elements of diagonal pre- and post compensators W_1 and W_2 such that the singular values of W_2GW_1 are desirable. This means high gain at low frequencies, roll-of rate of approximately 20dB/decade at unit gain crossover with higher roll-off rates at higher frequencies. The loop shaping is done without explicit regard for the nominal plant phase information. A simple way of obtaining a diagonal precompensator is to use PI-controllers as the diagonal elements, and use the SIMC PID-tuning rules for the controller gain tunings.

4. Robustly stabilize the shaped plant W_2GW_1 using the formulas of the previous section. First, calculate the maximum stability margin $\epsilon_{max} = 1/\gamma_{min}$. Good robustness typically means $\epsilon_{max} > 0.25$. If the margin is too small, modify the compensators W_1 and W_2. It is easier to get good margins if the slope at unit gain crossover is kept reasonable (≈ -1). Chose a γ about 10% larger than γ_{min} and calculate the suboptimal controller K_∞.

5. Analyze the design. The desired loop shape is specified by W_1GW_2. After the inclusion of K_∞, the actual loop shape is given by $W_1K_\infty W_2G$ at plant input and $GW_1K_\infty W_2$ at plant output. It is therefore possible that the inclusion of K_∞ in the open-loop transfer function will cause deterioration in the open-loop shape specified by W_1GW_2. McFarlane and Glover (1990) show that the degradation in the loop shape is limited at frequencies where the specified loop shape is sufficiently large or sufficiently small. In particular, ϵ can be interpreted as an indicator of the success of the loop shaping in addition to providing a robust stability guarantee for the closed-loop system. A small value of ϵ_{max} always indicates incompatibility between the specified loop shape, the nominal plant phase, an d robust closed-loop stability.

   Check that the controller gain is kept reasonable without large overshoots and saturation, this check is easiest performed using simulations.

6. Implement the controller. The configuration in Figure 5.6 is useful, because references to not directly excite the dynamics of K_∞ (derivative kick).

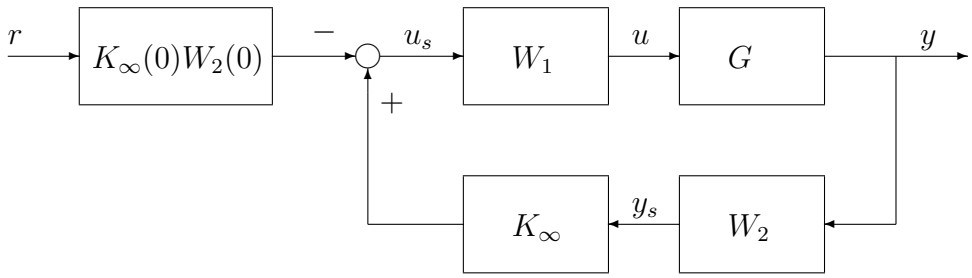

Figure 5.6: Practical implementation of the loop shaping controller

Note that, in contrast to the classical loop shaping approach, the loop-shaping here is done without explicit regard for the plant phase information, closed-loop stability is disregarded at this stage and only elementary loop-shaping principles are needed. Also, the robust stabilization is done without explicit frequency weighting, frequency dependent performance/stability trade-off is obtained implicitly through the loop shaping step. This makes the design procedure both simple and systematic.

6. Distillation Control

In the following an H_∞ loop shaping controller is designed for the high-purity distillation column. A dynamic model was derived for the column in chapter 3. This model is now used when designing the controller.

6.1 The control problem

A principal drawing of a distillation column system is shown in Figure 6.1. It contains a series of trays that are placed along its length. The liquid in the column flows over the trays from top to bottom while the vapor rises from bottom to top. (The experimental column is packed, not trayed, but this is unimportant at this stage.) The contact between the vapor and liquid facilitates a mass transfer between the phases. This interchange increases the concentration of the more volatile component in the vapor going up, while simultaneously increasing the concentration of the less volatile component in the liquid falling down.

The raw material, the *feed*, enters the column at a rate F with composition z_F. The top product, the *distillate*, is condensed and removed as liquid at a rate D with composition y_d. The bottom product, the *bottoms*, is removed as liquid at a rate B with composition x_b. The operation of the column requires that some of the bottoms is reboiled at a rate V to ensure the continuity of the *vapor* flow. Similarly, some of the distillate is refluxed to the top of the column at a rate L to ensure the continuity of the *liquid* flow.

The main controlled variables are the compositions y_d and x_b. In addition the holdups M_d and M_b must be controlled to avoid overflow. The manipulated variables are the internal flows L and V, and the external flows B and D. The feed rate F and composition z_F are considered as disturbances. (Often pressure is considered a controlled variable and the coolant flow a manipulated variable. Here we only consider total condensers and no direct pressure control.)

A control configuration must be chosen for the distillation column; i.e. which inputs are used to control which outputs. Normally two manipulated inputs are chosen for composition control. The holdups M_d and M_b are controlled with two SISO controllers using the remaining manipulated variables.

The LV configuration (i.e. L and V are used for composition control) is the only

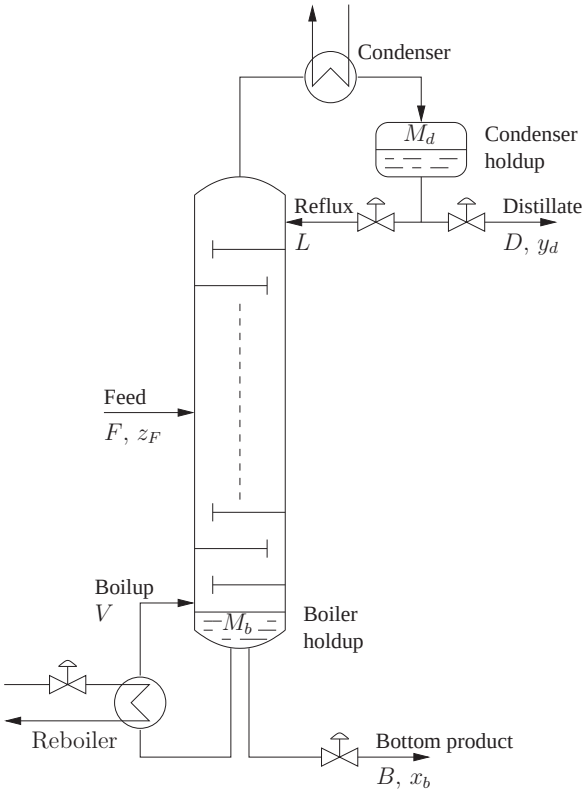

Figure 6.1: The distillation column system. Manipulated variables: L, V, B, D. Controlled variables: y_d, x_b, M_d, M_b. Disturbances: F, z_F

configuration considered here, mainly because this is one of the more frequent industrial configurations, which is known to work reasonably well. Other used configurations are the DV configuration or ratio configurations like (L/D)(V/B). Different configurations have different properties with regards to e.g. input uncertainty, feed disturbances and dynamic considerations. Controllers using the LV configuration are typically sensitive to input uncertainty (especially inverse based controllers) and feed disturbances. However, manipulating L and V directly favors a fast initial dynamic response. This is probably one of the main reasons for the popularity of the LV configuration. See e.g. (Skogestad and Morari, 1987; Kjellerhaug, 1988) for more on properties of different control configurations.

One of the control difficulties in the high purity distillation system is the ill-conditioned gain at different input directions (Skogestad et al., 1988). Increasing both of the internal streams L and V leads to higher product purities x_b and y_d. This move is along the weak input direction; the product compositions are quite insensitive to a simultaneous increase (or decrease) in both internal flows. On the other hand there is a large gain if the internal flows are moved along the complementary direction; increasing one internal stream while reducing the other stream will cause the product purities to change by a large amount in

opposite directions, i.e. one product purity increases while the other decreases.

Uncertainty makes control of ill-conditioned systems difficult. There are always uncertain model parameters dependent on operating points, frequency dependent, time varying or other. Sensors and actuators are imperfect, giving rise to uncertainty on the manipulated inputs implemented on the plant. For tight control of ill-conditioned plants the controller should try to compensate for the strong directionality by applying large input signals in the directions where the plant gain is low. However, because of uncertainty, the direction of the large input may not exactly correspond to the low plant-gain direction, and the amplification of these large input signals may be much larger than expected from the model. This will result in large values of the controlled variables, leading to poor performance or instability. An implication is that it may be difficult to significantly increase the closed-loop bandwidth of an ill-conditioned plant. Increasing the bandwidth requires high actuator usage, which is undesirable because of uncertainty.

6.2 Design specifications

The column operating point for this design was chosen at $y_d = 0.97$, $x_b = 0.01$, which is close to the center of the estimator calibration set (see Chapter 4). The column is separating a binary mixture of water and methanol ($z_F = 0.31$ corresponding to 50vol%) at a feed rate of 3.6 l/hour. The operating conditions are summarized in Table 6.1.

Table 6.1: Column operating conditions

Inputs	Compositions
Feed: 1.0ml/s	$y_d = 0.97$
Reflux: 0.52ml/s	$x_b = 0.01$
Boiler: 1.68kW	$z_F = 0.3095$

The design objectives are:

1. The controlled column should remain stable for input gain perturbations of up to ±50% (±6dB) and time delays of up to 30 seconds on each input.

2. No steady state offset.

3. The control action should not be oscillatory, and have little overshoot as this may cause flooding.

4. The response to steps in reference signals should be realistically fast, with no controller saturation during transients.

5. Good disturbance attenuation.

The input uncertainty in the design objectives is chosen because the inputs are believed to be the most important uncertainty factors. There is a physical time delay in the pipes from the reflux drum to the top of the column, and from applying voltage to the heating coils to actual temperature increase in the coils and increased vapor rate. The input/output characteristics of the pumps and heating coils are also uncertain, giving input gain uncertainties.

6.3 Linear system models

The nonlinear model from chapter 3 is described by the equations

$$\dot{x} = f(x, u_L, u_V, F, z_F); \qquad x \in \mathbb{R}^{26} \tag{6.1}$$
$$y = g(x, u_L, u_V, F, z_F); \qquad y \in \mathbb{R}^2, \tag{6.2}$$

where the volumetric reflux flow u_L and the boiler power u_V are used as inputs instead of the molar flows L and V. Model outputs $y = [Y_d, X_b]^T$ are logarithmic compositions

$$Y_d = \ln(1 - y_d); \quad X_b = \ln(x_b), \tag{6.3}$$

which are known to linearize the initial dynamic response of the column. This model was linearized numerically around the operating point given in Table 6.1 and reduced from 26^{th} order to 8^{th} order using balanced truncation model reduction. The order of the synthesized H_∞ controller is equal to the order of the plant plus the order of the pre- and post-compensators, and using a reduced order plant model prevents high controller order. When the linear model was reduced to less than 8^{th} order, the differences between the full- and reduced-order model frequency responses increased markedly, and it was decided not to reduce the model below eight order.

In Figure 6.2 is shown a step response in the nonlinear and the low order linear models. The input step size is approximately 1% of the nominal value, and the difference between the nonlinear and the linear models is small. The difference of course becomes smaller with smaller steps. In Figure 6.3 is shown a similar step response, but now with a step size ten times bigger . The nonlinear dynamics clearly becomes more dominating, especially for steps in boilup, and steady state errors becomes rather large. Nevertheless, initially, say the first 40 minutes, the linear and the nonlinear models still follow each other closely.

The SIMC-PI tuning rules requires a first-order plus delay model. Skogestad (2004) describes how to obtain a first-order model from a higher order transfer function, however he does not discuss how to deal with complex zeros or poles and his proposed model-reduction method was therefore not used. Instead the full order linear model was excited with white noise, and the input-output data (u_L, Y_d) and (u_V, X_b) was used to identify parameters in two first-order plus delay transfer function models between the column inputs u_L and u_V and the logarithmic distillate and bottoms compositions respectively.

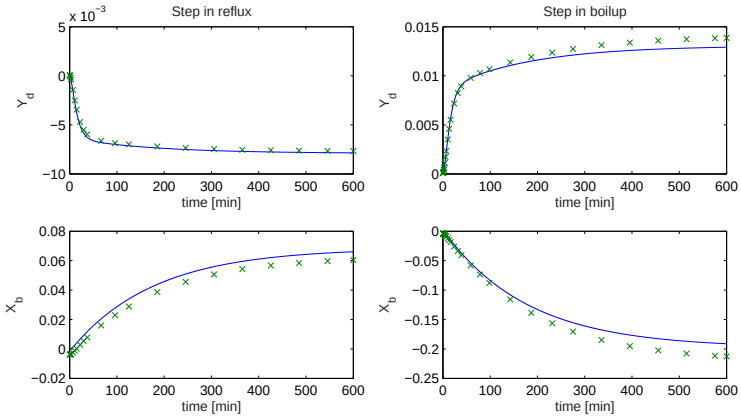

Figure 6.2: Step response with step size 1% of nominal values. Solid line: linear model; +: nonlinear model. Left plots: step in reflux flow; right plots: step in boilup.

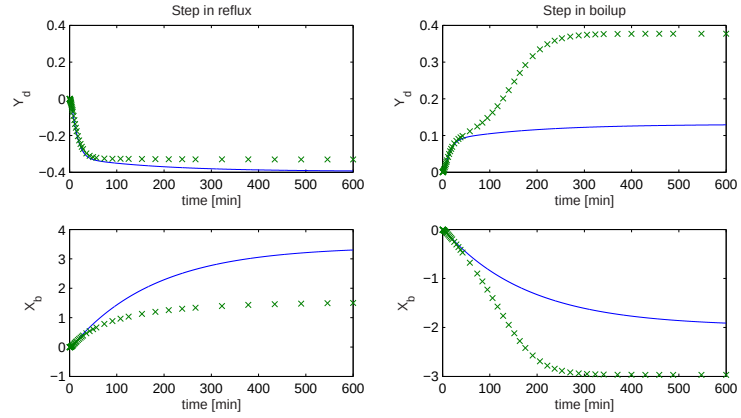

Figure 6.3: Step response with step size 10% of nominal values. Solid line: linear model; +: nonlinear model. Left plots: step in reflux flow; right plots: step in boilup.

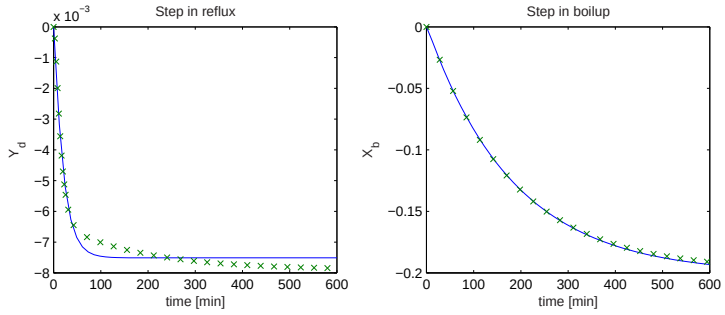

Figure 6.4: Response to step in input. Step size is 1% of nominal values. Solid line: first order plus delay linear model; +: 26^{th} order linear model. Left plot shows response to step in reflux flow, Right plot shows response to step in boilup.

Parameter identification was done using the Matlab System Identification Toolbox, which contains a method for directly identifying process models with dead time to input-output data. This gave the transfer function models

$$g_{11}(s) = \frac{-20.6}{19.6s+1}\mathrm{e}^{-1.49s}; \qquad Y_d(s) = g_{11}(s)u_L(s) \tag{6.4}$$

$$g_{22}(s) = \frac{-145}{184s+1}\mathrm{e}^{-1.52s}; \qquad X_b(s) = g_{22}(s)u_V(s) \tag{6.5}$$

The time constant for the bottoms composition is almost ten times as large as the time constant for the distillate composition. The physical explanation is that the bottoms holdup is about ten times larger than the reflux drum holdup, and the outputs are the compositions of the product flows leaving the boiler and the reflux drum. There is therefore a mixing tank effect, which is bigger for the bottoms product because of the larger bottoms holdup.

There is no explicitly modeled time delay, the delays in the first order models of approximately 1.5 minutes, is there because of the model reduction. In other words, the time delay acts as an approximation of the faster modes of the high order model. The slowest mode of the high order model is located at $p_1 \approx -0.005$ min^{-1}, with a corresponding time constant of $\tau_1 = -1/p_1 \approx 200$ minutes, which is close to the time constant in g_{22}. The high order transfer function between u_L and Y_d has a zero at $z_1 = -0.007\text{min}^{-1}$, which nearly cancels the slowest mode, p_1. The next slowest mode, $p_2 = -0.1\text{min}^{-1}$, with a corresponding time constant of $\tau_2 = 10$ minutes, is in the same order of magnitude as the time constant in g_{11}. The slowest zero between u_V and X_b is at $z_2 \approx 0.1\text{min}^{-1}$ and does not cancel the slow pole p_1 in the same way as what happens for the top composition.

The first order model for the bottoms, g_{22}, correlates well with the output from the higher order models, which clearly is dominantly a first order process when applying small steps (see Figure 6.4). The top composition response with step in reflux is more difficult

to recreate with a first order model, but the initial response, which is more important for control purposes, is still captured.

6.4 Controller design

We now have all which is needed to design the control system, and we can step through the prescriptive design procedure in the previous chapter. Two controllers will be designed, a conventional diagonal PI-controller, and an H_∞ loop shaping controller, where PI-controllers are used as loop shaping pre-compensators.

The inputs and outputs of the model are scaled by dividing each input by its maximum allowed input change (the distance to closest saturation limit), and dividing each output by a largest allowed control error corresponding to $\Delta y_d = \Delta x_b = 0.005$. More on different scaling methods is given in (Skogestad and Postlethwaite, 1996). (The gains in g_{11} and g_{22} are already scaled, a reverse scaling was done for the simulations in Figure 6.4.)

The system is as diagonal as possible with u_L and u_V as the first and second input respectively, and Y_d and X_b as the first and second output respectively.

The post-compensator, W_2, for the loop shaping is chosen as the identity matrix. The pre-compensator is chosen as

$$W_1 = \text{diag}(w_{top}, w_{bot}) = \begin{bmatrix} K_{c11}\left(\frac{\tau_{I11}s}{\tau_{I11}s+1}\right) & 0 \\ 0 & K_{c22}\left(\frac{\tau_{I22}s}{\tau_{I22}s+1}\right) \end{bmatrix}, \tag{6.6}$$

where K_{cii} and τ_{Iii} are selected according to the SIMC-PI tuning rules; equations (5.18) and (5.19), for the models $g_{11}(s)$ and $g_{22}(s)$ respectively. The compensator increases the low frequency gain and the crossover frequency can be moved by adjusting the tuning parameter τ_c for controller gains.

When using only the pre-compensator (PI control), the tuning parameter was selected to $\tau_c = 0.5\theta$ giving an integral time of approximately 9 minutes in both w_{bot} and w_{top}. With the robustifying H_∞ controller wrapped around the compensated plant (see Figure 5.6), the precompensator could be made more aggressive. A tuning value of $\tau_c = -0.5\theta$ (integral time of 3 minutes) for w_{top} and $\tau_c = 0$ (integral time of 6 minutes) for w_{bot} was found to yield a good controller in the simulations.

The maximum uncertainty bound with this loop-shape was $\epsilon_{max} = 1/\gamma_{min} = 0.41$, and a robustifying controller K_∞ was calculated for $\gamma = 1.1\gamma_{min}$. The singular values of the linear system model, G, the output loop transfer function with pure PI control, GW_1, and the robustified output loop transfer function, GW_1K_∞, are shown in Figure 6.5(a). Figure 6.5(b) shows the singular values of the prefilter, W_1, and the feedback part, K_∞. The pre-compensator, consisting of two PI-controllers, acts to increase the loop gain at low frequencies, giving good performance and disturbance attenuation. K_∞ alters the loop shapes around the cross-over frequency to improve stability with respect to plant

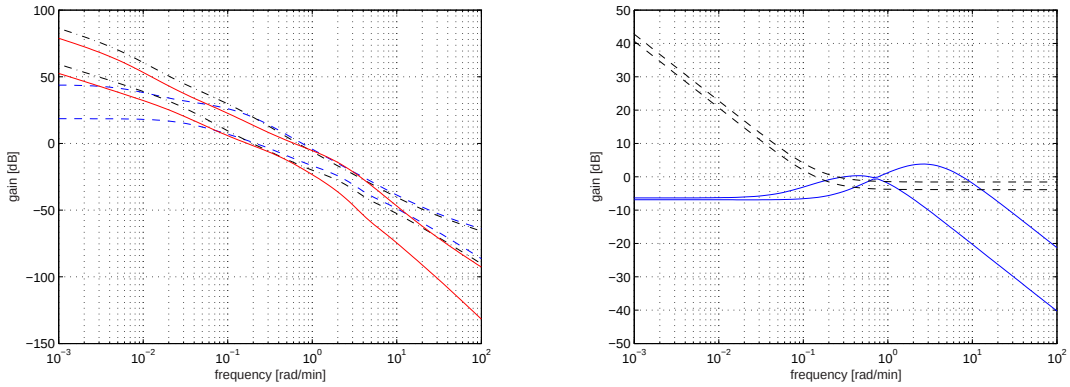

(a) Loop singular values. Solid line: GW_1K_∞; Dash dot line: GW_1; Dashed line: G.

(b) Controller singular values. Solid line: K_∞; Dashed line: W (PI-controller)

Figure 6.5: Singular value plots

parameter variations, and improves noise attenuation because of larger roll off at high frequencies.

From the singular value plots one would expect the PI-controller and the H_∞ loop shaping controller to perform similar on the nominal plant model, since the PI-compensator specifies the desired performance and the low frequency loop shapes are pretty much unchanged by including K_∞ in the feedback path. The H_∞ controller should give a closed loop system less affected by model perturbations, and also yield better noise rejection.

6.5 Simulations

Simulations were performed using the nonlinear column model with nominal plant parameters and with the four combinations of $\pm 50\%$ input gain perturbations with an input time delay of 0.5 minutes. The reference values were filtered with a first order filter with a time constant of five minutes to prevent high initial control action. Figure 6.6 and Figure 6.7 show the output response to a small step change in the distillate and bottoms composition references respectively. Figure 6.8 and Figure 6.9 show the response of the column to a step change in the feed flow rate and in the feed composition respectively.

Nonlinearities are more important when moving further away from the nominal operating point, and changes the plant behavior. This is illustrated in Figure 6.10 with larger reference steps and nominal input gain and delay.

The simulations clearly demonstrates that the H_∞ controller is less sensitive than the PI controller to plant parameter variations. In the nominal case, and close to the linearization point, the performance for the two controllers is similar, but the H_∞ controller generally yields better decoupling.

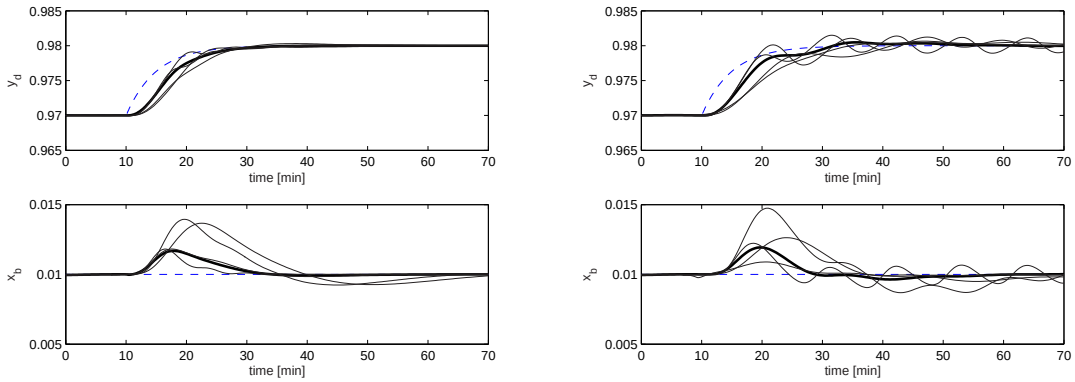

Figure 6.6: Step in y_d^{ref}. Dashed line: reference; thin solid line: response with plant perturbations; thick solid line: nominal response. Left plots: H_∞ controller; right plots: PI controller

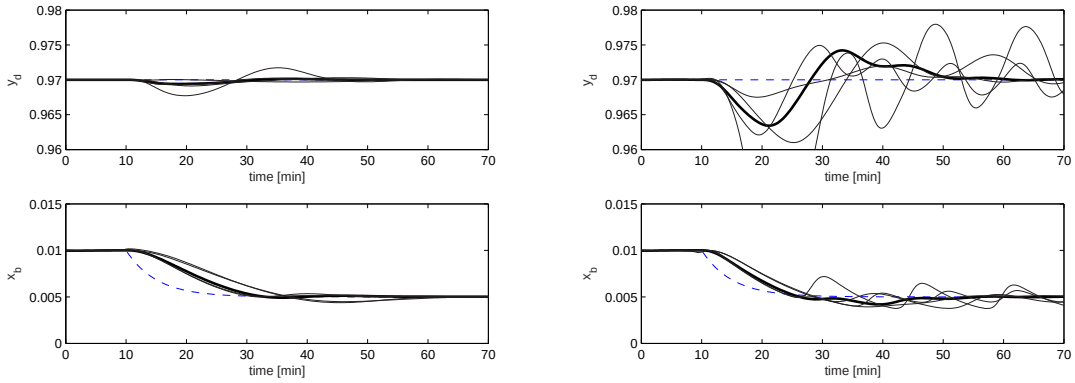

Figure 6.7: Step in x_b^{ref}. Dashed line: reference; thin solid line: response with plant perturbations; thick solid line: nominal response. Left plots: H_∞ controller; right plots: PI controller

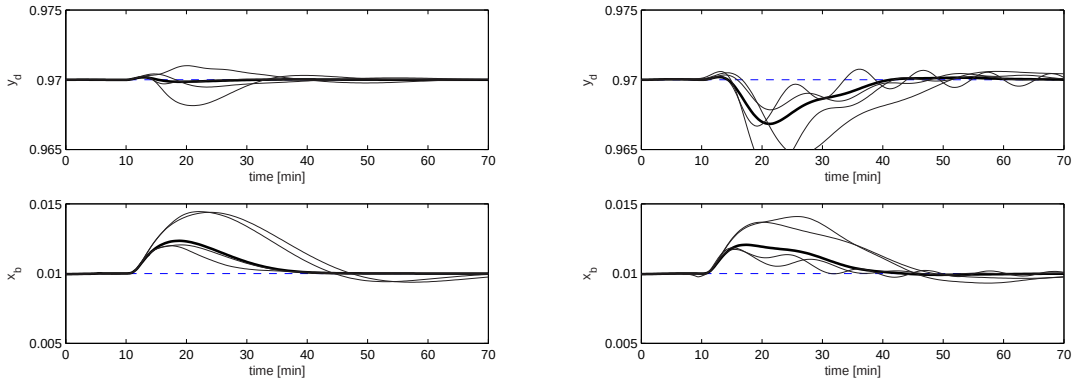

Figure 6.8: Step in feed rate from $F = 1\text{ml/s}$ to $F = 1.3\text{ml/s}$. Dashed line: reference; thin solid line: response with plant perturbations; thick solid line: nominal response. Left plots: H_∞ controller; right plots: PI controller

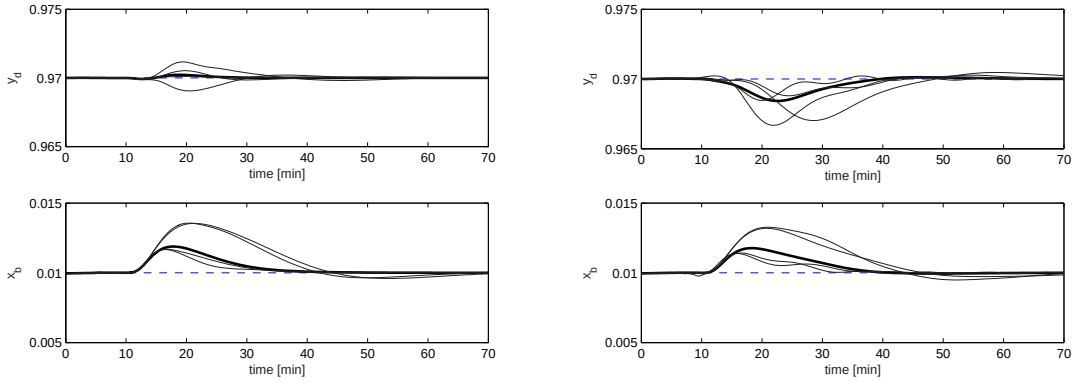

Figure 6.9: Step in feed composition from $z_f = 0.3$ to $z_f = 0.4$. Dashed line: reference; thin solid line: response with plant perturbations; thick solid line: nominal response. Left plots: H_∞ controller; right plots: PI controller

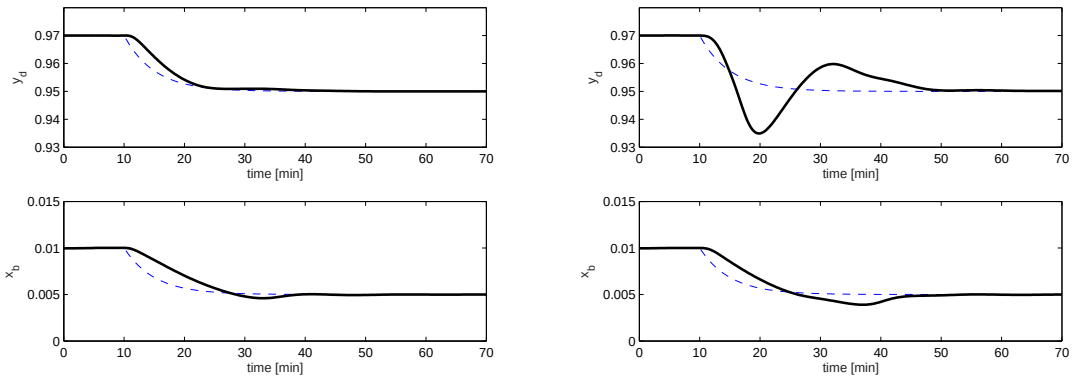

Figure 6.10: Big step in x_b^{ref} and y_d^{ref}. Dashed line: reference; solid line: output response. Left plots: H_∞ controller; right plots: PI controller

6.6 Experimental results

The controllers designed with the simulation model were implemented in LabView and connected to the experimental column. The controller gains were left unchanged from the simulations, but for the PI controller a measurement noise filter was necessary to obtain a smoother control signal, also giving less oscillations in the controlled variables. The noise filter was implemented as a 5^{th}-order filter with cut-off frequency $w_c \approx 20$rad/min, one tenth of the sampling frequency. The H_∞ controller showed, as expected from the steeper controller gain roll-off at high frequency, less sensitivity to high frequency noise and needed no additional signal filtering.

The experimental column was brought to steady state around the nominal operating point with $y_d = 0.97$ and $x_b = 0.01$. Then composition references were changed around the nominal values to demonstrate the performance of the system with the two different controllers. Figure 6.11 shows the controlled variables with the H_∞ controller. Figure 6.12 shows the outputs with the diagonal PI-controller.

Feed composition and feed rate were changed one at a time to see how the controllers reject disturbances. Figure 6.13 shows the response to disturbance step changes using the H_∞ controller. Figure 6.14 shows the response to disturbance step changes using the diagonal PI-controller. To better show the trend lines, the composition estimates are filtered in these figures.

There are only small differences in performance between the two controllers. The top composition is better with the H_∞ controller when far from the nominal operating point, showing less oscillations than the PI controller when going to $y_d = 0.95$, which again demonstrates better robustness to plant parameter changes. There also seems to be less coupling between the compositions with the H_∞ controller when changing the bottom composition, but the coupling is probably affected by initial conditions, y_d is not completely steady for neither of the controllers when stepping the bottoms reference.

The H_∞ controller on the other hand shows more variations in x_b than the PI controller, and also slower responses. The response in x_b to references and disturbances with the H_∞ controller appears somewhat sluggish with slower and larger oscillations. This was also seen in the simulations with low gain in the bottoms pre-compensator, w_{bot}. Different controller tunings may change the picture, but the H_∞ controller bandwidth cannot be significantly increased without entering the cut-off region of the noise filter found necessary with PI control. Thus, an H_∞ controller with more aggressive tunings will become more affected by noise.

Disturbance steps are not exactly equal for the two experimental runs. The steps in feed composition were performed by pouring some methanol into the feed tank, and then later pour some water into the feed to come back to the original composition. The actual feed composition changes were found afterwards by analyzing the feed samples with a pycnometer. Because of the higher feed methanol content it was necessary to reduce the feed rate in the experiment with the H_∞ controller to avoid saturation in the reflux pump.

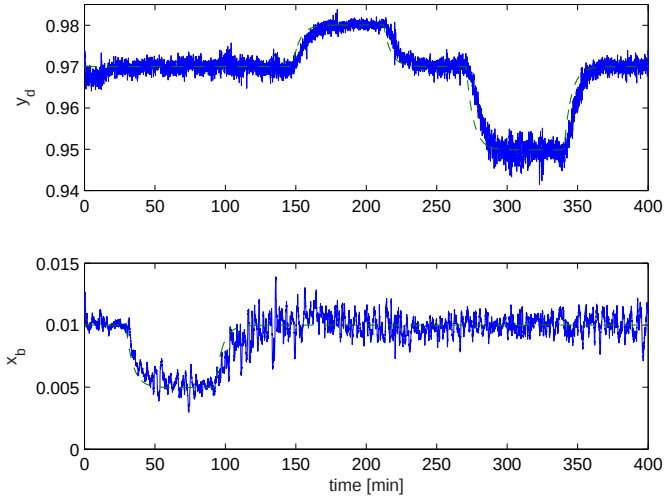

Figure 6.11: Experimental response to changes in composition references with the H_∞ controller. Solid line: composition estimate (unfiltered); dashed line: reference value.

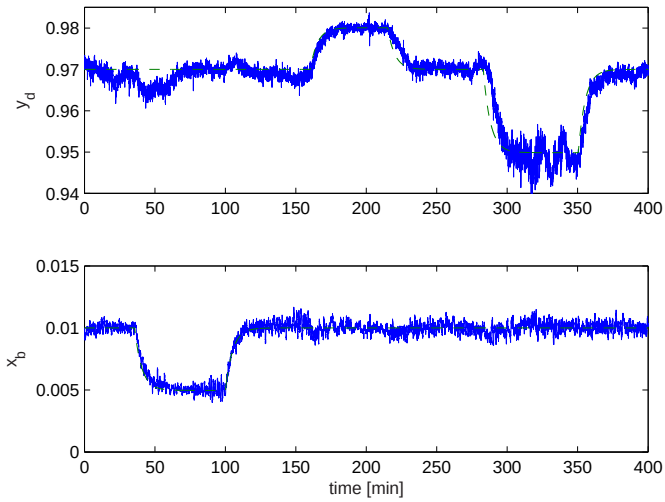

Figure 6.12: Experimental response to changes in composition references with the diagonal PI-controller. Solid line: composition estimate (unfiltered); dashed line: reference value.

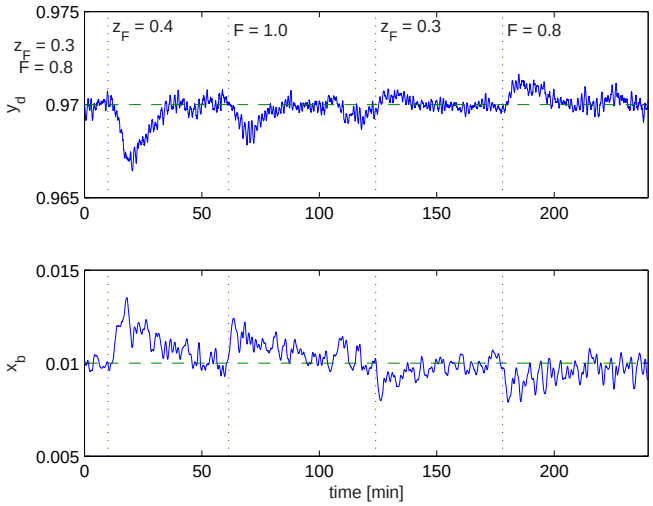

Figure 6.13: Experimental response to step changes in feed rate and feed composition with the H_∞ controller. Initially $F = 0.8$ml/s and $z_F = 0.3$ and the vertical lines show time of change of disturbances. First feed composition is increased to $z_F = 0.4$, then feed rate is increased to $F = 1.0$ml/s etc. Solid line: composition estimate (filtered); dashed line: reference value.

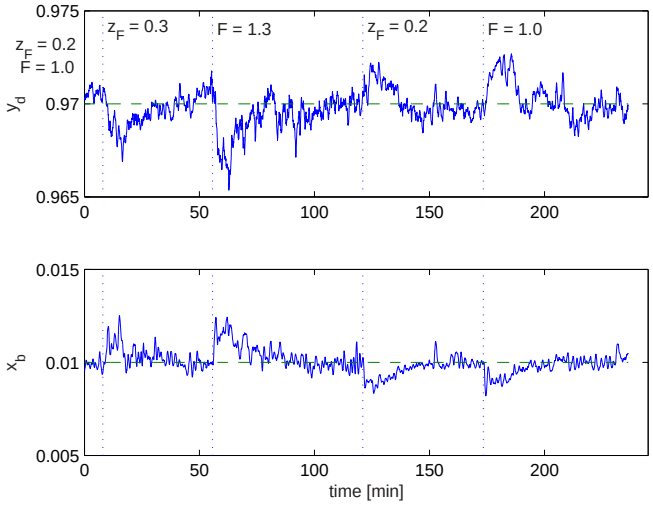

Figure 6.14: Experimental response to step changes in feed rate and feed composition with the diagonal PI-controller. Initially $F = 1$ml/s and $z_F = 0.2$ and the vertical lines show time of change of disturbances. First feed composition is increased to $z_F = 0.3$, then feed rate is increased to $F = 1.3$ml/s etc. Solid line: composition estimate (filtered); dashed line: reference value.

6.7 Discussion

Because of the static composition estimator, composition changes seem faster on the experimental column than in simulations. The bottoms composition estimate is only dependent on temperature measurements close to the boiler, which change quite fast when changing the vapor rate. Similarly, the distillate composition estimate is only dependent on temperatures in the top section of the column and respond fast to reflux rate changes. The actual composition of the product flows probably does not change as fast as the estimator claims, but this predictive property of the estimator reduces the effective delay between inputs and outputs and allows for apparently faster composition changes experimentally than what is achieved in simulations.

Another difference found between the simulation model and the experimental column is that more reflux was used experimentally, the total reflux rate was typically two to three times as high. Of course the nominal rates are dependent on factors like feed rate and composition, but these model inputs were changed quite a bit without the reflux rate reaching the level reached in experiments. With the experimental reflux and vapor rate values applied to the model, the model yielded higher distillate purity, and product samples analyzed with pycnometer showed the same thing ($y_d > 0.99$). Although it is difficult to accurately measure the composition of high purity methanol with a pycnometer, the method is good enough to conclude that the composition estimator is not very accurate. The estimator, basically giving out a weighted average of temperature measurements, is however good enough when the purpose is to stabilize the column.

An additional explanation for the discrepancy between required reflux in simulations and experiments is an inaccurate pump characteristic. After the experiments were finished, we had problems with the pump not pumping any reflux even at full speed, and this problem may have started gradually. Right now, the reason for this pump deficiency is not known, but it may be because the pump tube has been damaged or perhaps been squeezed somewhat out of position. Also, air may have become trapped in the pump, but we have tried to vent the tubes, and the problem persists.

Because especially the PI controller performs as good as it does experimentally, the simulated worst case parameter variations seem restrictive. On the other hand high-frequency noise and uncertainties were not even simulated, and it turned out that a low-pass filter was necessary in the experiments for the PI controller to perform satisfactory. It turned out to be difficult to simulate the system with measurement noise, the simulation step size decreased to zero and the simulation stopped when adding noise, even when using a stiff solver. Robustness could of course have been tested more rigorously both in simulations and also experimentally by adding artificial perturbations. However, the overall goal was to design an acceptable controller for the experimental column. Both of the controllers control the experimental column quite well, and are thus, one may argue, robust enough.

After all, there is little reason to use the H_∞ controller instead of the PI controller

on the experimental column. The difference in performance is just too small to justify using the more complex H_∞ controller. In simulations the H_∞ controller is more robust to plant parameter changes than the PI controller, but this level of robustness is hardly necessary when running the column close to a nominal operation point, which is normally the case. The PI controller is both much simpler to implement and to possibly re-tune online in case of changes in operation conditions (the re-tuning would on the other hand perhaps not be necessary with the more robust H_∞ controller). Another, and perhaps more important reason for choosing the PI controller, is the transition between manual and automatic control. With the 2×2 H_∞ controller, both composition loops are closed simultaneously and the column must be quite steady when turning on automatic control. With the PI controller, this is less important. Instead of closing both loops, the operator closes one loop, waits for the column to settle, and then closes the other loop. With some training, neither of the controllers are difficult to turn on, but for the unpracticed operator, the switch from manual to automatic PI control is less prune to failure than the switch to H_∞ control.

7. Conclusion

7.1 Experimental setup

Generally, the experimental setup works quite well. It is unfortunate that the temperature sensors are placed in a way which makes it difficult to replace them in case of sensor failure. Also the measurement range of the flow meters is somewhat above the actual flow rates, this in combination with pulsating flows, makes the flow meters not suitable for controller feedback if more accurate flow control is desired. They do however provide meaningful feedback in terms of flow visualization to the operator.

Lately there has been a problem with the reflux pump not pumping anything at all, and the bottoms pump tube has been replaced once because of a hole in the tube. One may argue that this is just the way it is with experimental equipment, it goes to pieces and does not cooperate when you need it the most. However, the broken bottoms pump tube was easily replaced, and replacing the reflux pump tube will hopefully solve the problem with the reflux as well.

7.2 Column model

The derived column model gives a good description of the experimental column, and simulations with the non-linear column model match well with experimentally obtained data. Obtaining the nominal holdup and the time constant for the linearized tray hydraulics was straightforward using a step in the reflux flow to excite the temperature dynamics. The obtained parameter values for the linearized tray hydraulics in the top section correlates well with reported values in articles. The parameter values does not correlate with reported values in the bottom section, which may be because of the sub-cooled feed creating a pinch region affecting the dynamic coupling between the top and the bottom sections.

7.3 Composition estimator

The estimator suffers from few parallels in the calibration data and few temperature measurements in the column. The estimator is good enough to use for stabilizing the column, but the accuracy is dubious to say the least. In particular, it has been verified using a pycnometer, that the distillate flow is purer than what the estimates says.

The predictive property of the static estimator reduces the effective delay between internal flow changes and composition estimates. The estimates are a likely to be a little ahead of actual composition changes, although this has not been experimentally verified. The reduced delay makes control easier.

7.4 Controller design

Simulations show that a conventional PI controller design can be made significantly more robust to parameter variations if adding an H_∞ controller in the feedback loop. Seen from a different perspective, the SIMC PI tuning rules are quite useful when calculating a pre-compensator in the H_∞ loop shaping technique.

Experimentally there is little difference in performance with the PI-controller, if including a noise filter, and the H_∞ loop shaping controller. The PI controller is preferred for its lower complexity and because the operator can close one loop at a time, making the transition from manual to automatic control easier.

7.5 Further work

The column is ready to be used as it is, but further improvements can be made especially on the composition estimator. The plan is to keep the column here at NTNU for a little longer to test it out with other operators than the author. As of now, the only one who know the control program and its user interface is the author. A detailed manual is in progress to explain and document the LabView control program, and hopefully give some useful hints to the new operator running the system.

References

Choe, Y. and W. Luyben (1987). Rigorous dynamic models of distillation columns. *Ind. Eng. Chem. 26*, 2158–2161.

de Jong, S. (1993). Simpls: An alternative approach to partial least squares regression. *Chemometrics and Intelligent Laboratory Systems 18*, 251–263.

Doyle, J. C. and G. Stein (1981). Multivariable feedback design: Concepts for a classical/modern synthesis. *IEEE Transactions on Automatic Control AC-26*(1), 4–16.

Fredenslund, A., J. Gmehling, and P. Rasmussen (1977). *Vapor-liquid equilibria using UNIFAC*. Elsevier.

Geankoplis, C. (1993). *Transport Processes and Unit Operations* (3 ed.). Prentice Hall.

Glover, K. and D. McFarlane (1989). Robust stabilization of normalized coprime factor plant descriptions with $\mathcal{H}_\infty$-bounded uncertainty. *IEEE Trans. Automat. Contr. 34*(8), 821–830.

Gmehling, J. and U. Onken (1977). *Vapor-Liquid Equilibrium Data Collection: Aqueous-Organic Systems*, Volume I. DECHEMA.

Green, M. and D. Limebeer (1995). *Linear Robust Control*. Prentice Hall.

Kjellerhaug, P. (1988). Regulering av destillasjonskolonne. Master's thesis, NTH.

McFarlane, D. and K. Glover (1990). *Robust controller design using normalized coprime factor plant descriptions*. Number 138 in Lecture notes in control and information sciences. Berlin: Springer.

Mejdell, T. (1990). *Estimators for product compositions in distillation columns*. Ph. D. thesis, NTH.

Naes, T. and H. Martens (1985). Comparison of prediction methods for multicollinear data. *Communications in Statistics, Simulations and Computations 14*(3), 545–576.

Reppe, I. (2004). Modellering og estimering av destillasjonskolonne. Prosjektrapport fordypningsemne, NTNU.

Safonov, M., D. Limebeer, and R. Chiang (1989). Simplifying the $\mathcal{H}_\infty$ theory via loop-shifting, matrix-pencil and descriptor concepts. *International Journal of Control 50*(6), 2467–2488.

Sinnot, R. (1999). *Chemical engineering design* (3 ed.), Volume 6 of *Coulson & Richardson's Chemical Engineering*. Butterworth Heinemann.

Skogestad, S. (1997). Dynamics an control of distillation columns - a critical survey. *Modeling, Identification and Control 18*, 177–217. Reprint of paper from *IFAC-symposium DYCORD+'92*, Maryland, Apr. 27-29, 1992.

Skogestad, S. (2004). Simple analytic rules for model reduction and pid controller tuning. *Modeling, identification and control 25*(2), 85–120.

Skogestad, S. and M. Morari (1987, October). Control configuration selection for distillation columns. *AIChE Journal 33*(10), 1620–1635.

Skogestad, S. and M. Morari (1988). Understanding the dynamic behaviour of distillation columns. *Ind. Eng. Chem. Res. 27*, 1848–1862.

Skogestad, S., M. Morari, and J. Doyle (1988, December). Robust control of ill-conditioned plants: High-purity distillation. *IEEE Transactions on Automatic Control 33*(12), 1092–1105.

Skogestad, S. and I. Postlethwaite (1996). *Multivariable Feedback Control*. John Wiley & Sons.

Wittgens, B. (1999). *Experimental Verification of Dynamic Operation of Continous and Multivessel Batch Distillation Columns*. Ph. D. thesis, NTNU.

Zhou, K. and J. C. Doyle (1998). *Essentials of robust control*. New Jersey: Prentice Hall.